


New zircon ages on the Cambrian–Ordovician volcanism of the Southern Gemicum basement (Western Carpathians, Slovakia): SHRIMP dating, geochemistry and provenance

Anna Vozárová¹  · Nickolay Rodionov² · Katarína Šarinová¹ · Sergey Presnyakov²

Received: 7 July 2016 / Accepted: 3 November 2016 / Published online: 24 November 2016
© Springer-Verlag Berlin Heidelberg 2016

Abstract The Southern Gemicum basement in the Inner Western Carpathians, composed of low-grade volcano-sedimentary rock complexes, constitutes a record of the polyphase Cambrian–Ordovician continental volcanic arc volcanism. These metavolcanic rocks are characterized by the enrichment in K, Rb, Ba, Th and Ce and Sm relative to Ta, Nb, Hf, Zr, Y and Yb that are the characteristic features for volcanic arc magmatites. The new SHRIMP U–Pb zircon data and compilation of previously published and re-evaluated zircon ages, contribute to a new constrain of the timing of the Cambrian–Ordovician volcanism that occurred between 496 and 447 Ma. The following peaks of the volcanic activity of the Southern Gemicum basement have been recognized: (a) mid-late Furongian at 492 Ma; (b) Tremadocian at 481 Ma; (c) Darriwilian at 464 Ma prolonged to 453 Ma within the early Upper Ordovician. The metavolcanic rocks are characterized by a high zircon inheritance, composed of Ediacaran (650–550 Ma), Tonian–Stenian (1.1–0.9 Ma), and, to a lesser extent, Mesoproterozoic (1.3 Ga), Paleoproterozoic (1.9 Ga) and Archaean assemblages (2.6 Ga). Based on the acquired zircon populations, it could be deduced that Cambrian–Ordovician arc crust was generated by a partial melting of Ediacaran basement in the subduction-related setting, into which old crustal fragments were incorporated. The ascertained zircon inheritances with Meso-, Paleoproterozoic

and Archaean cores indicate the similarities with the Saharan Metacraton provenance.

Keywords Western Carpathians · Cambrian–Ordovician arc volcanism · U–Pb zircon geochronology · Geochemistry · Provenance

Introduction

The essential part of the Early Palaeozoic complex occurrences in the Southern Gemicum Unit (SGU) is formed by the volcanic sedimentary formations, which underwent the regional metamorphism under P–T of the lower greenschist facies (Sassi and Vozárová 1987; Faryad 1991; Vozárová 1993a; Molák and Buchardt 1996). This complex is referred to as the Gelnica Group (GG) that was first defined and regionally delimited in the geological map of the Slovenské rudohorie Mts., 1:50,000—eastern part (Bajaník et al. 1984). The GG sedimentary sequence has several volcanogenic horizons within three stratigraphic levels. Thus, “in situ” U–Pb SHRIMP zircon dating has been applied, with the main objective to prove the age of volcanism and to specify the stratigraphy of the SGU low-grade basement. The accepted isotopic age of the GG metavolcanic rocks was, for the first time, documented from the locality Helcmanovce, by “in situ SIMS” dating on SHRIMP II equipment (St.-Petersburg, VSEGEI), at 482 ± 6 Ma (Putiš et al. 2008). Later, the zircon populations from nine samples of the three lithostratigraphic units of the GG rock complex have been analysed. The set of more than 140 zircon SHRIMP data confirmed the two phase late Cambrian–Ordovician volcanic events, with concordia ages of 492 and 464 Ma, respectively (Vozárová et al. 2010). In spite of many zircon age data, some

✉ Anna Vozárová
vozarova@fns.uniba.sk

¹ Department of Mineralogy and Petrology, Faculty of Natural Sciences, Comenius University in Bratislava, Mlynská dolina Ilkovičova 6, 842 15 Bratislava 4, Slovak Republic

² Centrum of Isotopic Research (CIR), All-Russian Geological Research Institute (VSEGEI), Sredny Prospekt 74, St.-Petersburg, Russia 199 106

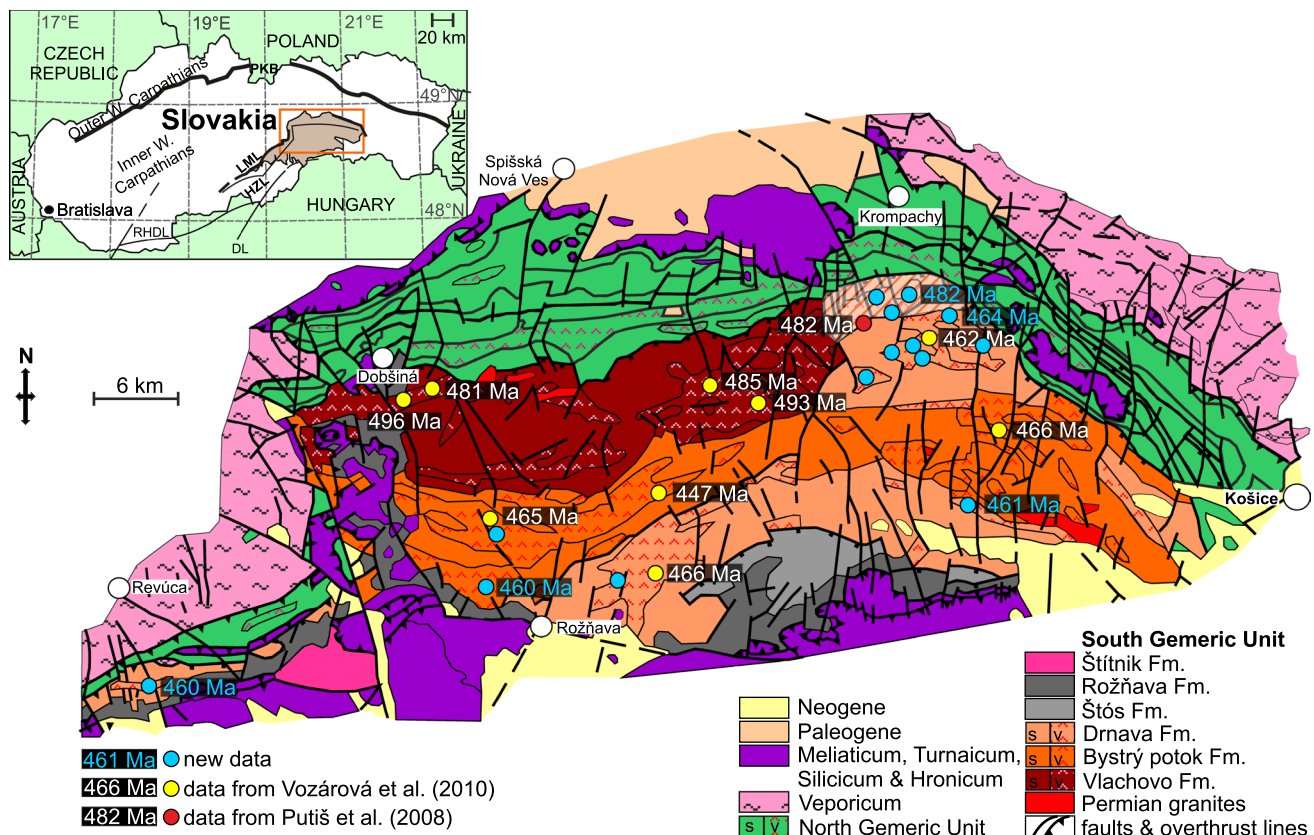


Fig. 1 Geological sketch of the Southern Gemic Unit (SGU) showing the localities of magmatic zircon samples (modified according to the geological map of Slovakia, 1/50,000, Biely et al. 1996b). NE part of the Drnava Fm. contains zircons with the similar ages as

zircons from the Vlachovo Fm. Thus we consider this part to be redefined and added to the Vlachovo Fm—the striped part in the Fig. 1. Abbreviations: *s* metasediments; *v* metavolcanics

problems were still not resolved, e.g. discrepancy between zircon SHRIMP ages from the locality of Helcmanovce (482 Ma, Putiš et al. 2008) and its enlisting to the youngest Drnava Formation (after Bajaník et al. 1984). Therefore, the further five samples were collected from the two upper lithostratigraphic units of the GG sequence to find a better regularity of the collected age data (Fig. 1). Consequently, the main topic of investigation was focused on indisputably confirmation of the existence of the first and second volcanic phase in the entire late Cambrian–Ordovician time span.

Geological background

The Western Carpathians are the northernmost east–west trending belt of the European Alpine range, linked to the Eastern Alps in the west and to the Eastern Carpathians in the east. The Western Carpathian orogenic belt consists of several northward-stacking crustal-scale super units and several cover nappe systems (Andrusov 1968; Maheľ 1986; Biely et al. 1996a, b; Rakús et al. 1998 and references

therein; Plašienka et al. 1997). This orogenic belt is traditionally divided into the Outer Western Carpathians (OWC) and Inner Western Carpathians (IWC) (Andrusov 1968; Maheľ 1986; Biely et al. 1996a, b; Plašienka et al. 1997; Rakús et al. 1998 and references therein) (Fig. 1). The main differences between them are the timing of the Alpine nappe emplacement and the intensity of related deformational and metamorphic events. The OWC contains the Cenozoic (pre-Miocene) rootless nappe complexes which overthrust various units of the European platform (Janik et al. 2011). The IWC comprises pre-Late Cretaceous nappe structures and rock complexes recording the high-pressure and low-temperature (HP/LT) Late Jurassic subduction events, and the Early to middle Cretaceous collision deformation and metamorphism. The Pieniny Klippen Belt (PKB) marks the boundary between these two structural zones (Fig. 1; Biely et al. 1996a, b and references therein). Fragments of the Variscan crust with their post-Variscan sedimentary cover were incorporated into the early to middle Cretaceous tectonic units of the internal zone of the Western Carpathians orogenic system. Each such unit consists of a crystalline basement

and a characteristic Upper Palaeozoic/Mesozoic envelope sequence (Tatricum, Northern and Southern Veporicum, Zemplinicum, Northern and Southern Gemericum). Generally, Upper Palaeozoic sedimentary complexes are also present in the basal part of several rootless nappes (Hronicum, Meliaticum, Turnaicum and Silicum), consisting mainly of Mesozoic complexes. The Tertiary transform fault, Rába–Hurbanovo–Diosjenő Line (RHDL; Matura et al. 2000) separates the Western Carpathians from the Carnic–Dinaridic type Pelso Megaunit (Haas 2001) that is located south from the investigated SGU area. In its easternmost prolongation, the RHDL transform fault line continues into the system of Darnó Line (DL), which represents the Tertiary contact between the Southern Gemericum, Meliaticum, and Pelso Megaunit.

The SGU belongs to the innermost part of the Alpine Western Carpathians and as a whole it clearly overrides the Northern Gemericum Unit (NGU) along the tectonic contact that is represented by the Hrádok–Železník Line in the west (HZL; defined by Abonyi 1971), which continues to the east into the system of thrust faults (Fig. 1). During the pre-Gosau period (Santonian–Campanian) the NGU and SGU units were amalgamated and widely overthrust on the Veporicum Unit, coursing at the present surface the Lubeník–Margecany Line (LML, Fig. 1) (Biely et al. 1996b). The polystage Cretaceous convergence of the Gemericum and Veporicum units is marked by a strong shortening of the both NGU and SGU units and development of the several thrust zones (e.g. HZL, LML) that interacted by the forthcoming transpressional shearing (Trans-Gemer Shear Zone in sense Lexa et al. 2003).

The major part of the SGU basement is formed by the low-grade Early Palaeozoic volcanic sedimentary sequence of the Gelnica Group (GG). Three lithostratigraphic units have been identified within the GG, from the bottom to upwards, designed as the Vlachovo (VF), Bystrý potok (BPF) and Drnava (DF) formations (Snopko and Ivanička in Bajaník et al. 1983, 1984) (Fig. 1). The further extended pre-Permian low-grade complex is the Štós Formation that is located only in the SE part of the SGU basement (Fig. 1). There is tectonic contact between the Gelnica Group and the Štós Formation rock complexes. A shallow north-verging thrust plane is documented by the deep seismic profile (Vozár et al. 1995). Both pre-Permian low-grade crystalline complexes are unconformably overstepped by the Permian continental sediments of the Gočaltovo Group (Fig. 1), associated with the Kungurian acid volcanic rocks (273 ± 3 Ma and 275 ± 3 Ma U–Pb zircon ages; Vozárová et al. 2009). Equally, the SGU crystalline basement was penetrated by the Permian granites (monazite ages ranging from 276 to 263 Ma—Finger and Broska 1999; Finger et al. 2003; Re–Os molybdenite data of 262 and 264 Ma—Kohút and Stein 2005; U–Pb zircon data 277 and 257 Ma—Radvanec et al. 2009).

Due to the intensive Early/Middle Cretaceous stacking and thrusting of the Inner Western Carpathians nappe units, the SGU rock complexes were affected by the strong Alpine structural and metamorphic overprinting (Bajaník et al. 1983; Lexa et al. 2003; Dallmayer et al. 2005; Vozárová et al. 2014).

Gelnica Group lithostratigraphic features

The GG was generally described as a megasequence of the deep-water turbidite siliciclastic sediments, associated with the volcanic/volcaniclastic rocks of prevalent rhyolite–dacite composition (Snopko 1967; Snopko and Ivanička 1978; Snopko and Ivanička in Bajaník et al. 1983). Marginal and distal turbidity facies were distinguished in the GG megasequence. Distal facies are accompanied with the thin lenses of lydites and allodapic limestones. The acid to intermediate magmatic arc volcanism (Vozárová and Ivanička 1996) was highly explosive, which resulted in the redeposition of a vast amount of volcanoclastic material into the fore-arc basin by the gravity and mass flow current systems (Vozárová 1993b). Various sized fragments of rhyolite–dacites to andesites were mass-transported together with pyroclastic rocks. Besides them, thin horizons of metabasaltic volcanoclastics and sparse metabasalts bodies occur. Olistoliths of metabasalts were incorporated in the binder of gravity sliding and slumping. Their chemical composition signalizes mixed tectonic settings of magmatic source, with chemical character similar to continental arc basalts, island arc basalt, mid-oceanic ridge basalts and enriched mid-oceanic ridge basalts (Ivan 1994).

The GG associations of facies represent various parts of the marine slope/rise complex graded to the deep-sea plain. The slope and upper fan facies are composed of thick sequences of hemipelagic metapelites that have been cut by slumps and thick channels, filled with the metasandstones, metaconglomerates and metapyroclastics. The middle fan facies are characterized by smaller distal fan channels, which were filled with metasandstones, metapyroclastics, and carved up by planar laminated turbidites, lydites and allodapic carbonates in deep-sea plain.

The palynological analysis demonstrated the Cambrian–Ordovician to Early Devonian age of the GG sediments (Čorná and Kamenický 1976; Snopková and Snopko 1979; Ivanička et al. 1989). Further biostratigraphical data, based on the agglutinated foraminifers of the family *Psammospaeridae* and *Saccaminidae*, proved the Upper Cambrian/Ordovician age of the VF and the BPF sedimentary sequences (Vozárová et al. 1998; Soták et al. 1999). The first Cambrian/Ordovician U–Pb concordia magmatic zircon ages gave the 494 ± 1.6 Ma for the VF metavolcanites and 466 ± 1.5 and 464 ± 1.7 Ma for the BPF and DF metavolcanites,

respectively (Vozárová et al. 2010). These isotopic ages limited the former biostratigraphic data.

Method of investigation

The new geochronological data, using U–Pb sensitive high-resolution ion microprobe (SHRIMP II, CIR Laboratory of VSEGEI, St.-Petersburg) on zircons obtained from the five samples of the Southern Gemicum basement metavolcanic rocks are presented. Further fifteen bulk chemical analyses of metavolcanic rocks were completed.

The rock samples (Table 1) have been analysed for bulk chemical composition of the rock-forming oxides, rare earth and trace elements in the Bureau Veritas Commodities Canada Ltd. (former ACME Analytical Laboratories Ltd., Canada). Following a lithium metaborate/tetraborate fusion and dilute nitric digestion, major elements and trace and rare elements (REE) were analysed by mass spectrometry and (ICP-MS) and inductively coupled plasma emission spectrometry (ICP-ES). The analytical accuracy was controlled using geological standard materials and is estimated to be within the 0.01% error (1σ , relative) for major elements, and within the 0.1–0.5 ppm error range (1σ , relative) for trace elements and 0.01–0.05 ppm for REEs.

U–Pb in situ dating

Zircons have been extracted from rocks by standard grinding, heavy liquid and magnetic separation analytical techniques. The rock-forming minerals were studied by an electron microprobe (CAMECA SX-100, in the laboratory of the Geological Survey of Slovak Republic, Bratislava). The internal zoning structure of individual zircon crystals and shapes were analysed by CL images.

In situ U–Pb analyses were performed using sensitive high-resolution ion microprobe (SHRIMP II) in the Center of Isotopic Research (CIR) at VSEGEI, applying a secondary electron multiplier in peak-jumping mode following the procedure described by Williams (1998) and Larionov et al. (2004). The primary beam size allowed the analysis of ca. $27 \times 20 \mu\text{m}$ area. The $80 \mu\text{m}$ wide ion source slit, in combination with a $100 \mu\text{m}$ multiplier slit, allowed mass-resolution $M/\Delta M \geq 5000$ (1% valley); hence, all the possible isobaric interferences were resolved. The following ion species were measured in the sequence: $^{196}(\text{Zr}_2\text{O})$ – ^{204}Pb –background (ca. 204 AMU)– ^{206}Pb – ^{207}Pb – ^{208}Pb – ^{238}U – ^{248}ThO – ^{254}UO . Four cycles for each analysis were acquired. Each fifth measurement was carried out on the TEMORA Pb/U standard (Black et al. 2003). The 91,500 zircon (Wiedenbeck et al. 1995) was applied as “U-concentration” standard. The collected results have been processed by the SQUID v1.12 (Ludwig 2005a) and

ISOPLLOT/Ex 3.22 (Ludwig 2005b) software, with decay constants of Steiger and Jäger (1977). The common lead correction was done on the basis of measured $^{204}\text{Pb}/^{206}\text{Pb}$. The ages given in text, if not additionally specified, are $^{207}\text{Pb}/^{206}\text{Pb}$ for zircon older than 1500 Ma, and $^{206}\text{Pb}/^{238}\text{U}$ for those younger than 1500 Ma. The errors are quoted at 1σ level for individual points and at 2σ level in the concordia diagram, for concordia ages or any previously published ages discussed in the text. The relative probability plots were processed by ISOPLLOT/Ex 3.75 (Ludwig 2012) software.

Petrological and chemical characteristics of metavolcanic rocks

Petrography

The acid to intermediary metavolcanites is represented mostly by blastofelsitic and porphyritic varieties, in which phenocrysts constitute up to 30–40% of the rock volume. Among the phenocrysts quartz, Na–Ca feldspars (An_{5-10}) and micropertthitic K-feldspars are dominant. Nearly all the quartz phenocrysts show embayed and anhedral features. Euhedral and subhedral plagioclases usually exhibit albite twinning, but can include pericline and carlsbad twinning. Heterogeneous sericitization of the plagioclase phenocrysts is most common. The K-feldspars form the euhedral phenocrysts, often with carlsbad twinning. In the intermediary varieties, the magmatic biotite relics are frequent. Rarely, the “phantoms” after amphiboles have been noticed. Both mafic phenocrysts are replaced by chlorite and Fe-bearing oxides, but their original shape has been retained. Ilmenite and magnetite occur as small anhedral to subhedral microphenocrysts and as subhedral inclusions in former mafic phenocrysts. Microcrystalline and blastofelsitic groundmasses include very fine plagioclases, quartz, sericite, chlorite and Fe–Ti oxides. Apatite, zircon, rutile, monazite are frequent accessory minerals.

As it was mentioned above, the GG metavolcanics are associated with huge mass of the pyroclastic rocks, frequently with the well-preserved ignimbrite structure. They contain fragments of quartz, plagioclase and K-feldspar phenocrysts, as well as highly altered and deformed relics of biotite and amphibole. Comparing with the metavolcanic rocks they differ in distinct orientation of matrix, with higher concentration of sericite and/or chlorite and finally some Fe–Ti oxides.

The GG rocks were deformed during polyphase regional metamorphism. The former pre-Alpine metamorphic mineral assemblages, mainly within the GG metasediments, were overprinted and recrystallized during the Jurassic/Cretaceous tectonothermal events. Metamorphic monazite

Table 1 List of analysed metavolcanic samples with localization

| Sample no. | Lithostratigraphic unit | Sample locality | GPS coordinates |
|------------|-------------------------|---|----------------------------|
| GZ-2* | Vlachovo Formation | Starovodská dolina valley, 670 m a.s.l. | N48°47'130" E20°39'950" |
| GZ-6* | Vlachovo Formation | SW from Mníšek nad Hnilcom, 540 m a.s.l. | N48°47'517" E20°47'584" |
| G-1/10 | Vlachovo Formation | NW from Turzovské kúpele, NW from Gelnica town, 580 m a.s.l. | N48°51'666" E20°53'920" |
| G-2/10 | Vlachovo Formation | NW from Turzovské kúpele, NW from Gelnica town, 532 m a.s.l. | N48°51'665" E20°54'009" |
| GZ-4* | Vlachovo Formation | SE from Dobšiná town, 447 m a.s.l. | N48°47'910" E20°23'290" |
| GZ-5* | Vlachovo Formation | SE from Dobšiná town, 760 m a.s.l. | N48°47'510" E20°25'140" |
| G-8/10 | Vlachovo Formation | N from Helcmanovce village, 448 m a.s.l. | N48°50'287" E20°58'671" |
| GZ-37 | Vlachovo Formation | NW from Gelnica town, 527 m a.s.l. | N48°51'695" E20°54'028" |
| GZ-1* | Bystrý potok Formation | W from Gemerská Poloma village, 344 m a.s.l. | N48°42'480" E20°27'452" |
| GZ-1a* | Bystrý potok Formation | 10 m W from locality GZ-1 | N48°42'480" E20°27'452" |
| GZ-7* | Bystrý potok Formation | Starovodská dolina valley, 980 m a.s.l. | N48°44'500" E20°38'150" |
| GZ-9* | Bystrý potok Formation | SW from Kojšova Hoľa height, 1105 m a.s.l. | N48°46'400" E20°58'200" |
| GZ-15 | Bystrý potok Formation | NW from Rožňava town, SE slope of Turecká height, 473 m a.s.l. | N48°40'220" E20°29'059" |
| G-6/10 | Drnava Formation | SW from Gelnica town, 354 m a.s.l. | N48°50'853" E20°55'927" |
| G-7/10 | Drnava Formation | NW from Huta Matilda settlement, 500 m a.s.l. | N48°50'052" E20°53'929" |
| G-3/10 | Drnava Formation | S from Helcmanovce village, 819 m a.s.l. | N48°48'172" E20°51'812" |
| GZ-38 | Drnava Formation | SW part of Gelnica town, 373 m a.s.l. | N48°50'853" E20°55'927" |
| GZ-8* | Drnava Formation | Perlová dolina valley, 495 m a.s.l. | N48°49'600" E20°57'100" |
| GZ-3* | Drnava Formation | NW from Krásnohorské Podhradie village, S from Banský vrch height | N48°41'010" E20°38'518" |
| GZ-13 | Drnava Formation | N from Lucia Baňa settlement, 421 m a.s.l. | N48°43'813" E20°55'084" |
| GZ-14 | Drnava Formation | Turčocká dolina valley, NW from Rákoš village, 291 m a.s.l. | N48°37'333" E20°09'882" |
| GZ-16 | Drnava Formation | Pača village, 438 m a.s.l. | N48°41'014" E20°36'734" |
| GZ-17 | Drnava Formation | Krásnohorské Podhradie-Uhorná road-cut, 863 m a.s.l. | N48°41'241" E20°38'852" |
| G-5/10 | Drnava Formation | WNW from Prakovce village, 410 m a.s.l. | N48°49'134" E20°53'448" |

Samples with asterisks are taken from Vozárová et al. (2010)

ages in metavolcanites proved the dominant Early Cretaceous overprinting, with preserved relics of the Middle/Upper Jurassic events. The dominant age peaks were

recognized at 133–184 Ma, with a small peak at 100 Ma (Vozárová et al. 2014). The Jurassic ages nearly correspond with the $^{40}\text{Ar}/^{39}\text{Ar}$ data from the Meliaticum Unit

(150–170 Ma; Maluski et al. 1993; Faryad and Henjes-Kunst 1997, Dallmayer et al. 1996, 2005) and with the monazite ages from the SGU Permian volcanites (167 Ma; Vozárová et al. 2008). Further $^{40}\text{Ar}/^{39}\text{Ar}$ data from the Gemericum Unit and from the Gemer–Vepor contact zone are shifted to the 80–100 Ma Late Cretaceous ages (Dallmayer et al. 2005; Jeřábek et al. 2008; Putiš et al. 2009). Irregular foliated plains are mostly fine-grained, where foliation obliterated the initial rock texture. Fe–Ti oxides, Fe–Mg chlorite, albite and sericite crystallized along the foliation planes. The crenulation cleavage was partly recognized. The recrystallized quartz phenocrysts exhibit a mosaic-like texture, when the rocks are strongly foliated. Feldspar phenocrysts are broken and dominantly replaced by sericite. Scarce mafic phenocrysts (biotite and isolated amphibole) have been totally replaced by Fe–Mg chlorite and Fe–Ti oxides.

Geochemistry

New major, trace and rare earth elements data from the fifteen GG volcanic rocks are given in Table 2. The formerly acquired analytical data from the nine samples (Vozárová et al. 2010) are presented in the diagrams and Table 2 as well, and they are indicated by asterisks. As the most major elements are highly mobile (except Al_2O_3 , TiO_2 , P_2O_5) during regional metamorphism and super-imposed hydrothermal processes (Gibson et al. 1983; MacLean 1990), the high field strength elements (HFSE; Zr, Nb, Y) and TiO_2 were used for metavolcanic rocks classification. All the investigated samples have LOI contents of 0.7–3.9 wt%, suggesting secondary overprinting by various degrees of hydrothermal alteration and possible alkali's migration. The GG metavolcanic rocks have SiO_2 contents ranging from 61 to 78 wt%, and after Pearce (1996a) classification, they consist of rhyodacite and andesite composition of the sub-alkaline suite (Fig. 2a). Based on the Zr/Y ratios (Fig. 2b; after Barrett and MacLean 1994), the majority of andesitic samples show a transitional and calc-alkaline magmatic trend, with Zr/Y ratios between 4.5–7 and 7–25, respectively. The smaller group of rhyodacite samples indicate a tholeiitic-like character, with Zr/Y ratios between 2 and 4.5, approximately (Fig. 2b). Generally, the GG metavolcanic rocks display linear trends of decreasing TiO_2 , FeO_T , MgO , MnO , Al_2O_3 , P_2O_5 and CaO and increasing K_2O with increasing of SiO_2 (Table 2). Only Na_2O versus SiO_2 data are somehow scattered, which might be caused by the post-magmatic alkali rock alteration. The VF and DF metavolcanites are plotted from the andesite to rhyodacite fields, at which the BPF metavolcanites are strictly displayed in the andesite field.

The GG metavolcanic rocks present a light REE (LREE) enrichment with $\text{La}_N/\text{Yb}_N = 2.27\text{--}11.6$ for the VF, $\text{La}_N/$

$\text{Yb}_N = 6.97\text{--}9.20$ for the BPF and $\text{La}_N/\text{Yb}_N = 3.72\text{--}9.02$ for the DF metavolcanites (chondrite normalization after McDonough and Sun 1995). These also display variable Eu negative anomalies, with Eu/Eu^* values ranging from 0.09 to 0.72 for the VF, from 0.52 to 0.57 for the BPF and from 0.09 to 0.64 for the DF metavolcanic rocks (Fig. 3a). The negative Eu anomalies become more and more significant along with the fractional differentiation from andesite/dacite trough rhyodacite, indicating that plagioclase crystallization dominated during the magma evolution. All the patterns for differently fractionated rocks are parallel to each other with the similar tendencies (Fig. 3a).

In the primitive mantle-normalized spidergrams (after Sun and McDonough 1989; Fig. 3b), all the investigated samples are characterized by the enrichment in large ion lithospheric elements (LILE) such as K, Rb and Th, and the apparent negative anomalies of Sr and HFSE, such as Nb, Ta and Ti relative to the neighbouring elements. Ba and U contents are more scattered. In addition, the distribution patterns for the VF and DF metavolcanic rocks display the negative P anomalies, mostly in the more differentiated samples. On the contrary, nearly all the studied samples from the three lithostratigraphic units show the Pb positive anomalies. It is generally accepted that decreasing Sr and Ba contents with increasing of silica reflects fractional crystallization of plagioclases, while decreasing tendency of other incompatible elements, such as Nb, Ta, P, Ti may reflect fractionation of some minor and accessory phases (apatite, rutile, ilmenite) along with the magma evolution. Then a slight variability in distribution of elements could correspond with the gradual magma fractionation. The fractionated VF and DF metavolcanites are characteristic by large negative Eu anomalies (Fig. 3a). These large Eu anomalies are associated with the low Sr contents. Nevertheless, there is a linear correlation between Zr and Eu/Eu^* , which implies that feldspar and zircon crystallized throughout the evolution of this magmatic system (Fig. 4a). The decrease in Zr content from 182 to ~74 ppm in the VF metavolcanites and from 239 to 44 ppm in the DF metavolcanites requires the zircon fractionation. The increasing La/Sm_N chondrite ratios with Zr contents (Fig. 4c) can be explained by a fractionation of hornblende and apatite that fractionate REE (Sisson 1994; Heumann and Davies 1997). Negative correlations through decreasing of Zr with fractionation show the variation of SiO_2 and Rb/Sr ratios (Fig. 4b, d).

Additionally, the upper continental crust UCC-normalized trace elements plots (normalizing values after Taylor and McLennan revised by McLennan 2001) were used to interpret the chemical characteristic of the GG metavolcanic rocks. They have generally a flat UCC-normalized multi-elements patterns (Fig. 5) with depletion in Ti, Al, Sc, V ($\pm\text{Zr}$, Hf and Eu) and weakly negative Nb anomalies.

Table 2 Major and trace element concentrations in the Cambrian–Ordovician metavolcanic rocks

| Sample | Bystrý potok Fm. | | | | | | | | | | Drnava Fm. | | | | | | | | | |
|--------------------------------|------------------|--------|-------|-------|-------|--------|--------|--------|-------|-------|------------|-------|-------|-------|-------|--------|--|--|--|--|
| | GZ-1* | GZ-1a* | GZ-7* | GZ-9* | GZ-15 | G-6/10 | G-7/10 | G-3/10 | GZ-38 | GZ-8* | GZ-3* | GZ-13 | GZ-14 | GZ-16 | GZ-17 | G-5/10 | | | | |
| wt% | 63.68 | 66.15 | 67.27 | 68.63 | 66.70 | 78.16 | 75.59 | 77.08 | 75.94 | 75.39 | 61.07 | 63.24 | 65.56 | 66.96 | 67.42 | 70.57 | | | | |
| Al ₂ O ₃ | 17.93 | 16.40 | 15.25 | 14.69 | 14.75 | 11.71 | 12.56 | 11.57 | 12.26 | 12.19 | 17.72 | 14.96 | 15.86 | 15.10 | 14.14 | 15.19 | | | | |
| Fe ₂ O ₃ | 4.30 | 4.09 | 3.78 | 3.10 | 6.57 | 0.86 | 1.09 | 0.87 | 1.36 | 1.21 | 6.59 | 7.04 | 4.98 | 5.77 | 6.12 | 1.88 | | | | |
| MgO | 1.76 | 1.68 | 1.37 | 1.40 | 1.07 | 0.16 | 0.13 | 0.07 | 0.18 | 0.23 | 2.55 | 2.98 | 1.32 | 1.44 | 1.67 | 1.01 | | | | |
| CaO | 0.72 | 0.86 | 2.67 | 1.55 | 0.72 | 0.01 | 0.02 | 0.01 | 0.02 | n.d. | 0.64 | 1.65 | 2.34 | 0.43 | 0.77 | 0.18 | | | | |
| Na ₂ O | 3.70 | 4.77 | 4.00 | 4.82 | 0.31 | 1.78 | 1.46 | 0.82 | 2.81 | 0.40 | 4.31 | 2.92 | 3.41 | 3.16 | 2.46 | 3.22 | | | | |
| K ₂ O | 4.16 | 2.89 | 2.01 | 1.86 | 4.76 | 6.43 | 8.60 | 8.34 | 6.22 | 8.88 | 3.03 | 2.27 | 3.29 | 3.88 | 3.99 | 5.08 | | | | |
| TiO ₂ | 0.61 | 0.56 | 0.51 | 0.59 | 0.86 | 0.06 | 0.06 | 0.06 | 0.10 | 0.08 | 0.86 | 0.77 | 0.67 | 0.71 | 0.56 | 0.58 | | | | |
| P ₂ O ₅ | 0.210 | 0.185 | 0.195 | 0.173 | 0.120 | 0.020 | 0.030 | 0.020 | 0.040 | 0.035 | 0.250 | 0.180 | 0.150 | 0.190 | 0.180 | 0.130 | | | | |
| MnO | 0.02 | 0.03 | 0.05 | 0.04 | 0.09 | n.d. | n.d. | n.d. | 0.01 | n.d. | 0.06 | 0.08 | 0.04 | 0.05 | 0.07 | 0.01 | | | | |
| Cr ₂ O ₃ | 0.004 | 0.004 | 0.004 | 0.006 | 0.011 | 0.011 | 0.009 | 0.018 | n.d. | n.d. | 0.008 | 0.010 | 0.010 | 0.010 | 0.008 | 0.009 | | | | |
| LOI | 2.9 | 2.2 | 2.7 | 3.2 | 3.9 | 0.8 | 0.5 | 1.1 | 0.9 | 1.4 | 2.9 | 3.7 | 2.2 | 2.1 | 2.4 | 1.9 | | | | |
| Cs | 2.8 | 2.4 | 2.4 | 23.3 | 23.4 | 2.1 | 2.5 | 2.5 | 1.8 | 2.3 | 4.7 | 2.4 | 4.1 | 3.6 | 6.4 | 1.3 | | | | |
| Sc | 13 | 12 | 11 | 11 | 13 | 3 | 4 | 3 | 6 | 6 | 16 | 15 | 17 | 13 | 11 | 14 | | | | |
| Ba | 852.9 | 660.0 | 495.0 | 404.0 | 696.0 | 230.0 | 191.0 | 264.0 | 314.0 | 887.0 | 734.1 | 501.0 | 542.0 | 728.0 | 859.0 | 1792 | | | | |
| Ga | 22.2 | 22.5 | 20.9 | 20.5 | 17.7 | 10.7 | 13.8 | 10.3 | 13.8 | 14.6 | 21.6 | 17.6 | 17.2 | 18.1 | 18.3 | 14.5 | | | | |
| Hf | 6.8 | 7.1 | 6.4 | 5.6 | 10.0 | 2.9 | 3.8 | 2.7 | 4.2 | 3.9 | 6.4 | 5.8 | 5.5 | 6.3 | 6.4 | 6.2 | | | | |
| Nb | 14.2 | 12.5 | 13.3 | 10.8 | 15.5 | 6.4 | 6.5 | 8.2 | 7.2 | 7.6 | 13.6 | 11.0 | 11.6 | 12.7 | 12.6 | 10.5 | | | | |
| Rb | 132.4 | 93.3 | 67.8 | 69.6 | 231.3 | 127.4 | 196.2 | 184.1 | 169.4 | 197.7 | 127.1 | 102.3 | 96.0 | 123.5 | 142.0 | 92.8 | | | | |
| Sr | 48.0 | 87.6 | 313.7 | 124.9 | 27.4 | 12.3 | 19.8 | 13.4 | 21.4 | 12.3 | 134.9 | 122.4 | 212.2 | 75.9 | 102.2 | 27.3 | | | | |
| Ta | 0.9 | 0.9 | 0.9 | 0.8 | 1.1 | 1.0 | 1.2 | 1.1 | 1.0 | 1.0 | 1.0 | 0.8 | 0.8 | 1.0 | 0.9 | 0.8 | | | | |
| Th | 16.8 | 17.8 | 17.6 | 11.7 | 13.0 | 18.4 | 25.4 | 20.2 | 27.1 | 22.6 | 15.1 | 13.0 | 12.1 | 15.4 | 15.4 | 13.3 | | | | |
| U | 2.7 | 2.5 | 3.3 | 2.5 | 2.7 | 2.4 | 1.7 | 1.4 | 3.1 | 1.2 | 3.4 | 3.0 | 5.4 | 2.7 | 2.9 | 2.6 | | | | |
| V | 64 | 59 | 55 | 72 | 80 | n.d. | n.d. | n.d. | n.d. | n.d. | 93 | 91 | 89 | 80 | 63 | 42 | | | | |
| Zr | 228.6 | 215.0 | 205.1 | 171.3 | 340.5 | 63.7 | 74.6 | 67.4 | 107.9 | 84.9 | 239.9 | 208.3 | 196.6 | 224.1 | 215.5 | 226.9 | | | | |
| Y | 39.2 | 37.3 | 38.3 | 27.9 | 34.4 | 19.8 | 36.8 | 37.6 | 44.0 | 39.0 | 36.5 | 33.1 | 30.2 | 38.0 | 36.6 | 29.9 | | | | |
| La | 46.6 | 45.1 | 45.2 | 29.5 | 35.0 | 18.1 | 22.9 | 22.5 | 48.5 | 32 | 44.5 | 30.9 | 34.1 | 33.2 | 38.6 | 28.0 | | | | |
| Ce | 93.8 | 90.1 | 85.0 | 58.6 | 72.0 | 40.8 | 49.4 | 54.5 | 100.5 | 62.6 | 87.8 | 65.8 | 69.6 | 71.5 | 74.4 | 53.3 | | | | |
| Pr | 11.34 | 11.20 | 11.03 | 7.73 | 8.70 | 4.96 | 6.33 | 6.08 | 12.09 | 8.24 | 10.93 | 8.19 | 8.70 | 8.72 | 9.52 | 7.23 | | | | |
| Nd | 43.4 | 42.1 | 38.4 | 30.1 | 33.9 | 18.7 | 23.4 | 23.4 | 44.9 | 30.4 | 42.8 | 32.8 | 34.6 | 33.5 | 37.3 | 29.2 | | | | |
| Sm | 7.70 | 7.96 | 7.68 | 6.08 | 6.34 | 4.45 | 5.75 | 5.59 | 9.42 | 6.68 | 8.20 | 6.15 | 6.41 | 6.75 | 7.09 | 5.63 | | | | |
| Eu | 1.30 | 1.27 | 1.27 | 1.07 | 1.04 | 0.18 | 0.20 | 0.18 | 0.28 | 0.23 | 1.57 | 1.07 | 1.31 | 1.08 | 1.02 | 0.99 | | | | |
| Gd | 7.17 | 6.91 | 6.63 | 5.33 | 5.84 | 3.75 | 5.84 | 5.96 | 8.37 | 6.62 | 7.75 | 6.14 | 6.13 | 6.77 | 6.83 | 5.33 | | | | |
| Tb | 1.29 | 1.24 | 1.22 | 0.98 | 1.00 | 0.63 | 1.08 | 1.12 | 1.14 | 1.24 | 1.31 | 1.01 | 0.98 | 1.14 | 1.13 | 0.90 | | | | |

Table 2 continued

| Sample | Bystrý potok Fm. | | | | | | | | | | Drnava Fm. | | | | | | | | | |
|--------------------------------|------------------|--------|--------|--------|-------|--------|--------|--------|-------|-------|------------|-------|-------|-------|-------|--------|--|--|--|--|
| | GZ-1* | GZ-1a* | GZ-7* | GZ-9* | GZ-15 | G-6/10 | G-7/10 | G-3/10 | GZ-38 | GZ-8* | GZ-3* | GZ-13 | GZ-14 | GZ-16 | GZ-17 | G-5/10 | | | | |
| Dy | 6.99 | 6.20 | 5.98 | 5.25 | 5.75 | 3.76 | 6.61 | 6.64 | 7.84 | 6.58 | 7.23 | 5.90 | 5.56 | 6.54 | 6.05 | 5.34 | | | | |
| Ho | 1.28 | 1.42 | 1.51 | 1.03 | 1.19 | 0.75 | 1.36 | 1.38 | 1.45 | 1.57 | 1.28 | 1.13 | 1.11 | 1.29 | 1.23 | 1.08 | | | | |
| Er | 3.81 | 3.64 | 4.13 | 2.78 | 3.50 | 2.39 | 3.94 | 4.05 | 4.46 | 4.97 | 3.69 | 3.39 | 3.12 | 3.83 | 3.63 | 3.16 | | | | |
| Tm | 0.56 | 0.53 | 0.61 | 0.43 | 0.55 | 0.37 | 0.60 | 0.64 | 0.71 | 0.69 | 0.55 | 0.52 | 0.49 | 0.59 | 0.55 | 0.47 | | | | |
| Yb | 3.57 | 3.33 | 3.46 | 2.60 | 3.41 | 2.52 | 4.02 | 4.11 | 4.14 | 4.46 | 3.35 | 3.18 | 3.05 | 3.49 | 3.35 | 2.82 | | | | |
| Lu | 0.50 | 0.51 | 0.56 | 0.40 | 0.52 | 0.37 | 0.59 | 0.61 | 0.66 | 0.69 | 0.47 | 0.46 | 0.45 | 0.52 | 0.49 | 0.44 | | | | |
| Ni | 8.5 | 10.2 | 8.2 | 15.4 | 30.4 | 7.7 | 4.2 | 5.8 | 0.9 | 0.6 | 20.8 | 40.1 | 28.6 | 37.8 | 38.2 | 3.1 | | | | |
| Pb | 1.4 | 1.4 | 25.0 | 4.1 | 3.0 | 8.0 | 3.6 | 4.7 | 13.1 | 2.3 | 14.2 | 37.0 | 5.3 | 17.2 | 17.1 | 11.3 | | | | |
| Co | 7.2 | 7.6 | 6.4 | 8.7 | 4.5 | 0.5 | 0.6 | 0.7 | 1.6 | 1.2 | 12.0 | 10.6 | 10.3 | 10.2 | 8.7 | 5.0 | | | | |
| Eu/Eu* | 0.533 | 0.522 | 0.543 | 0.573 | 0.521 | 0.134 | 0.105 | 0.095 | 0.096 | 0.105 | 0.600 | 0.531 | 0.637 | 0.487 | 0.447 | 0.551 | | | | |
| Sm/La _N | 3.779 | 3.538 | 3.675 | 3.030 | 3.447 | 2.540 | 2.487 | 2.514 | 3.215 | 2.991 | 3.389 | 3.138 | 3.322 | 3.071 | 3.400 | 3.106 | | | | |
| La/Sm _{UCN} | 0.908 | 0.850 | 0.883 | 0.728 | 0.828 | 0.610 | 0.597 | 0.604 | 0.772 | 0.719 | 0.814 | 0.754 | 0.798 | 0.738 | 0.817 | 0.746 | | | | |
| La/Yb _N | 8.867 | 9.200 | 8.874 | 7.708 | 6.973 | 4.879 | 3.870 | 3.719 | 7.958 | 4.874 | 9.024 | 6.601 | 7.595 | 6.462 | 7.828 | 6.745 | | | | |
| Sm/Yb _N | 2.346 | 2.600 | 2.414 | 2.415 | 2.023 | 1.921 | 1.556 | 1.480 | 2.475 | 1.629 | 2.662 | 2.104 | 2.286 | 2.104 | 2.302 | 2.172 | | | | |
| Sample | Vlachovo Fm. | | | | | | | | | | | | | | | | | | | |
| | GZ-2* | GZ-6* | G-1/10 | G-2/10 | GZ-4* | GZ-5* | G-8/10 | GZ-37 | | | | | | | | | | | | |
| SiO ₂ | 76.19 | 73.91 | 77.21 | 75.00 | 78.54 | 73.68 | 64.32 | 65.51 | | | | | | | | | | | | |
| Al ₂ O ₃ | 12.74 | 12.13 | 12.29 | 12.47 | 11.44 | 13.24 | 16.95 | 17.89 | | | | | | | | | | | | |
| Fe ₂ O ₃ | 1.22 | 1.15 | 1.57 | 1.55 | 1.44 | 2.03 | 5.38 | 3.05 | | | | | | | | | | | | |
| MgO | 0.18 | 0.39 | 0.60 | 0.59 | 1.18 | 2.47 | 2.66 | 1.00 | | | | | | | | | | | | |
| CaO | 0.02 | 0.21 | 0.05 | 0.04 | 0.01 | 0.55 | 0.33 | 0.32 | | | | | | | | | | | | |
| Na ₂ O | 1.02 | 0.56 | 4.07 | 1.19 | 0.03 | 1.76 | 5.18 | 4.76 | | | | | | | | | | | | |
| K ₂ O | 7.91 | 9.23 | 2.36 | 7.27 | 4.41 | 2.97 | 1.55 | 3.67 | | | | | | | | | | | | |
| TiO ₂ | 0.07 | 0.07 | 0.07 | 0.11 | 0.27 | 0.22 | 0.55 | 0.68 | | | | | | | | | | | | |
| P ₂ O ₅ | 0.030 | 0.032 | 0.020 | 0.030 | 0.040 | 0.056 | 0.120 | 0.300 | | | | | | | | | | | | |
| MnO | 0.01 | 0.02 | 0.01 | 0.01 | n.d. | 0.03 | 0.07 | 0.04 | | | | | | | | | | | | |
| Cr ₂ O ₃ | n.d. | n.d. | 0.015 | 0.007 | n.d. | n.d. | 0.011 | 0.009 | | | | | | | | | | | | |
| LOI | 0.7 | 2.2 | 1.7 | 1.7 | 2.4 | 2.8 | 2.8 | 2.7 | | | | | | | | | | | | |
| Cs | 3.3 | 2.7 | 2.7 | 3.2 | 3.5 | 3.7 | 2.5 | 4.6 | | | | | | | | | | | | |
| Sc | 5 | 4 | 5 | 5 | 9 | 9 | 18 | 12 | | | | | | | | | | | | |
| Ba | 360.6 | 292.0 | 156.0 | 358.0 | 792.0 | 694.0 | 353.0 | 591.0 | | | | | | | | | | | | |
| Ga | 14.0 | 10.9 | 13.5 | 14.5 | 13.8 | 15.4 | 17.1 | 20.4 | | | | | | | | | | | | |
| Hf | 3.7 | 3.6 | 3.7 | 3.9 | 3.5 | 4.5 | 5.3 | 5.0 | | | | | | | | | | | | |

Table 2 continued

| Sample | Vlachovo Fm. | | | | | | | | | |
|----------------------|--------------|-------|--------|--------|-------|-------|--------|--------|--|--|
| | GZ-2* | GZ-6* | G-1/10 | G-2/10 | GZ-4* | GZ-5* | G-8/10 | GZ-37 | | |
| Nb | 7.7 | 7.2 | 7.0 | 8.4 | 7.1 | 6.9 | 10.4 | 8.1 | | |
| Rb | 169.2 | 165.8 | 92.7 | 165.3 | 177.3 | 76.8 | 62.1 | 127.7 | | |
| Sr | 48.5 | 12.0 | 36.4 | 15.6 | 2.1 | 42.7 | 114.7 | 49.7 | | |
| Ta | 1.1 | 1.2 | 1.0 | 1.2 | 0.7 | 0.9 | 0.8 | 0.5 | | |
| Th | 20.0 | 23.1 | 21.9 | 23.3 | 14.8 | 16.0 | 12.8 | 10.6 | | |
| U | 3.3 | 1.7 | 2.7 | 2.9 | 2.8 | 1.6 | 3.1 | 3.6 | | |
| V | n.d. | n.d. | n.d. | n.d. | 29 | 21 | 64 | 84 | | |
| Zr | 84.6 | 74.5 | 81.3 | 95.4 | 103.8 | 118.9 | 191.3 | 182.5 | | |
| Y | 43.6 | 41.4 | 39.9 | 48.0 | 32.1 | 45.3 | 24.1 | 16.6 | | |
| La | 16.3 | 27.5 | 24.8 | 19.7 | 31.0 | 42.0 | 26.3 | 30.1 | | |
| Ce | 36.6 | 55.7 | 59.1 | 55.0 | 64.3 | 82.0 | 62.2 | 63.4 | | |
| Pr | 4.16 | 7.30 | 6.63 | 5.34 | 7.74 | 10.7 | 6.36 | 6.34 | | |
| Nd | 16.1 | 26.6 | 24.3 | 20.6 | 27.3 | 39.9 | 23.1 | 23.2 | | |
| Sm | 4.10 | 6.18 | 6.00 | 5.25 | 5.41 | 8.37 | 4.60 | 4.18 | | |
| Eu | 0.14 | 0.22 | 0.21 | 0.26 | 1.21 | 0.91 | 0.86 | 1.03 | | |
| Gd | 5.16 | 6.28 | 6.06 | 6.19 | 4.87 | 7.59 | 4.30 | 3.56 | | |
| Tb | 1.18 | 1.13 | 1.16 | 1.22 | 0.90 | 1.33 | 0.74 | 0.48 | | |
| Dy | 7.67 | 6.16 | 6.97 | 7.86 | 4.77 | 7.03 | 4.24 | 3.47 | | |
| Ho | 1.56 | 1.55 | 1.45 | 1.74 | 1.13 | 1.65 | 0.90 | 0.65 | | |
| Er | 4.87 | 4.21 | 4.36 | 5.27 | 3.10 | 4.55 | 2.60 | 1.84 | | |
| Tm | 0.76 | 0.67 | 0.68 | 0.77 | 0.42 | 0.72 | 0.40 | 0.31 | | |
| Yb | 4.88 | 3.96 | 4.33 | 4.82 | 2.62 | 4.23 | 2.56 | 1.80 | | |
| Lu | 0.68 | 0.62 | 0.64 | 0.71 | 0.40 | 0.65 | 0.37 | 0.27 | | |
| Ni | 0.3 | 0.4 | 4.1 | 3.6 | 1.6 | 2.1 | 12.6 | 6.4 | | |
| Pb | 5.2 | 2.7 | 19.1 | 2.4 | 12.5 | 2.3 | 4.4 | 1.7 | | |
| Co | n.d. | 0.5 | 1.4 | 1.2 | 1.6 | 2.3 | 8.3 | 8.1 | | |
| Eu/Eu* | 0.093 | 0.108 | 0.106 | 0.139 | 0.719 | 0.348 | 0.589 | 0.814 | | |
| Sm/La _N | 2.483 | 2.779 | 2.581 | 2.343 | 3.578 | 3.134 | 3.570 | 4.497 | | |
| La/Sm _{UCN} | 0.596 | 0.667 | 0.620 | 0.563 | 0.860 | 0.753 | 0.858 | 1.080 | | |
| La/Yb _N | 2.269 | 4.718 | 3.891 | 2.776 | 8.038 | 6.745 | 6.979 | 11.360 | | |
| Sm/Yb _N | 0.914 | 1.698 | 1.507 | 1.185 | 2.246 | 2.153 | 1.954 | 2.526 | | |

* Analyses taken from Vozárová et al. (2010); n.d. (not determined)—sample under detection limit; La/Sm_N—chondrite normalization after McDonough and Sun (1995); La/Sm_{UCN}—normalization to upper continental crust after Taylor and McLennan revised by McLennan (2001)

A typical Th enrichment could be involved in slab metasomatism. Fluids were probably derived from dehydration of hydrous silicate minerals within the slab and/or from the sedimentary rocks atop it (Johnson and Plank 1999; Pearce and Peate 1995). The La/Sm ratios, normalized to UCC values show a linear trend, nearly with the correlation coefficient $r \approx 1$, equivalent to $\text{La}/\text{Sm}_{\text{UCN}} = 1$ (UCN = Upper Crustal Normalized). All samples demonstrate $\text{La}/\text{Sm}_{\text{UCN}} < 1$ and they likely come from a source that was depleted relative to the UCC. There are small differences between fractionated and non-fractionated metavolcanics as they range from 0.56 to 0.77 and from 0.72 to 1.08, respectively.

The incompatible trace elements Ta, Th and Yb were used as a geochemical index of tectonic setting, based on revised Pearce (1983) by Gorton and Shandl (2000) discrimination diagrams (Fig. 6a). In the revised Ta/Yb versus Th/Yb discriminant diagram for intermediate and felsic rocks, the GG metavolcanics are plotted strictly within the field of an active continental margin (ACM) that is characteristic for continental arc volcanics. They have a tendency to be plotted at a higher ratio end of Th/Yb axis. Relationships based on the Th/Ta versus Yb (after Gorton and Shandl 2000) fully support the presented ACM tectonic interpretation. The higher Th/Ta values, ranging from 15 to 21, clearly correspond with the arc volcanic rocks.

To distinguish the effect of fractional crystallization from the source composition, we have used a plot of Rb/Zr versus Nb (after Brown et al. 1984). Figure 6b shows only a slight increase of Rb/Zr ratios (from 0.32 to 2.7) at more or less constant Nb contents (10.4–14.2 ppm). This chemical course confirms the competence of the GG metavolcanites to the normal volcanic arc, with a mainly subduction-enriched magma source. Thus, the increasing of Rb/Zr ratios may be explained by the effect of zircon fractionation and growth. In Fig. 6b the fractionated and non-fractionated metavolcanites are clearly separated. The fractional crystallization of zircon displays a decreasing Zr content at nearly constant Nb concentrations in the more fractionated volcanic rocks.

U–Pb SHRIMP zircon dating

Zircon characteristics

Zircon grains are mostly medium in size (100–200 μm) with except of the sample *GZ-37* that contains larger zircons (300–400 μm). Generally, zircons are mostly prismatic and colourless or pink. Clear and transparent, long- and short-prismatic euhedral in shape, with aspect ratios of 1:4 which are dominant, but stubby crystals, with aspect ratios 1:2, are also present (Fig. 7a–e). Majority of zircon

grains display magmatic oscillatory growth zoning (regular or irregular), concentric and less of marginal sector type. The mode of the compositional zoning varies widely from bimodal successions of rich and poor trace element bands to the small compositional differences, with only faintly visible compositional zoning. CL images show that some grains are composite, with inherited cores surrounded by a new growth zonation. Commonly, the regular growth zoning is interrupted by the textural discontinuities. In many cases, the original growth zoning is resorbed and later succeeded by a newly growth-zoned zircon. These are separated from their rims by the irregular surfaces, sorting out the unzoned and/or chaotically zoned cores from the oscillatory growth-zoned rims. In some zircon grains, the modifications of their internal texture with disruption of growth oscillatory zoning (mosaic and convolute texture) have been observed. This process is probably connected with the post-magmatic and late-magmatic influences of the magmatically derived fluids (Schaltegger et al. 1997; Pidgeon 1992). The metamict zircon crystals are mainly present in the higher differentiated VF and DF metavolcanites.

Zircon age data

Bystrý potok Formation

The sample *GZ-15* from the BPF metavolcanites was used for the SHRIMP study. Eleven analytical points in 11 zircon grains yielded 9 concordant or slightly discordant ages with the discordance degree ranging between +7 and –11% (Table 3). The remaining two analytical points were omitted from the calculation because of more than 20% discordance. The common lead content, $^{206}\text{Pb}_c$, is low, usually accounting less than 0.4% of the measured ^{206}Pb . The U and Th content is variable moderate (125–658 and 28–163 ppm, respectively). Majority of the $^{232}\text{Th}/^{238}\text{U}$ ratios are low to moderate, mostly between 0.33–0.10, corresponding well with zircons crystallizing within igneous and late-magmatic conditions.

The Proterozoic ages have been obtained from two grains (Table 3): 1057 ± 14 Ma (point 8) and 595 ± 8 Ma (point 10), with a discordance D of –3 and 4%. The Proterozoic grains emphasize the significant role of the inherited, old crustal components that are similar to the ages of detrital zircons reported from the associated GG greywackes (Vozárová et al. 2012).

The remaining seven grains fall within the age interval of 453–513 Ma, with the $^{206}\text{Pb}/^{238}\text{U}$ concordia age of 460 ± 5 Ma (Fig. 8), corresponding to the Darriwilian (after ICS Chronostratigraphic Chart 2016). As the majority of the studied zircon grains had inherited cores, all the measured analytical points were situated within the oscillation growth-zoned rims.

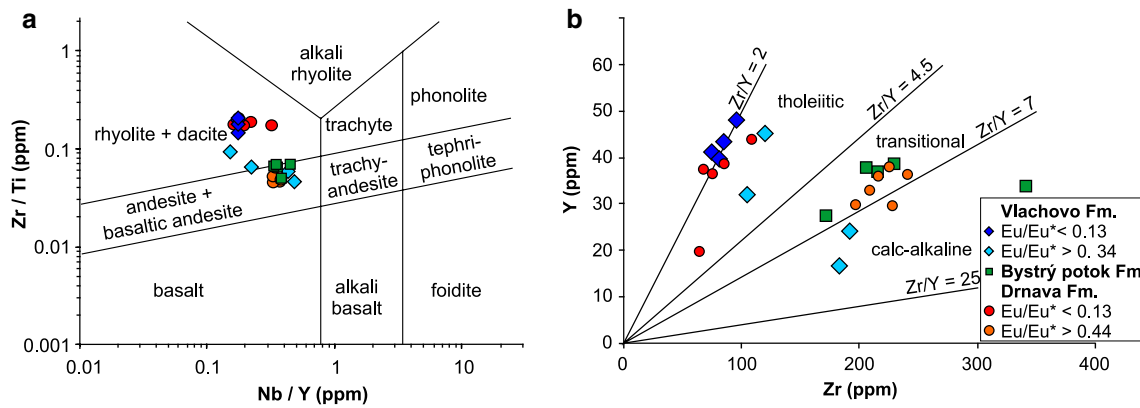


Fig. 2 a Distribution of the SGU metavolcanic rocks based on Zr/Ti versus Nb/Y after Pearce (1996a) diagram (revised Winchester and Floyd 1977), b Zr/Y magmatic affinity ranges for the SGU metavolcanic rocks (after Barrett and MacLean 1994)

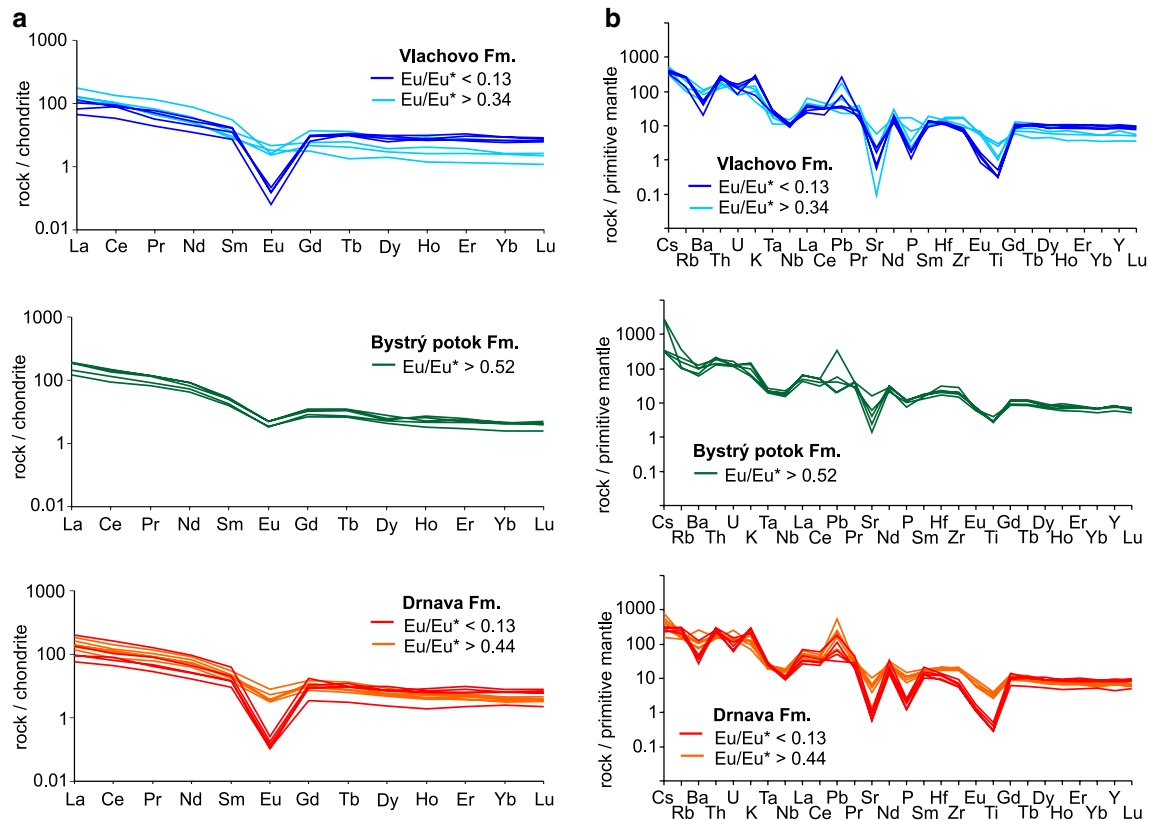


Fig. 3 a Chondrite-normalized REE distribution of the studied metavolcanic samples. Chondrite normalizing values after McDonough and Sun (1995), b primitive mantle-normalized incompatible element's diagram of the studied metavolcanites samples. Normalizing values after Sun and McDonough (1989)

Drnava Formation

Four samples were collected for the SHRIMP zircon dating from the DF metavolcanics (Table 1). Nevertheless, the acquired results were surprising and they document a discrepancy between the analytical age and lithostratigraphic

position of samples. The SHRIMP ages show that sample GZ-37, collected from the NE part of the DF occurrence, is older than the other three samples, GZ-38, GZ-13 and GZ-14, from E, S and SW part of the Drnava Formation (Fig. 1).

All 10 analytical points from nine zircon grains in the sample GZ-37 yielded concordant or slightly discordant

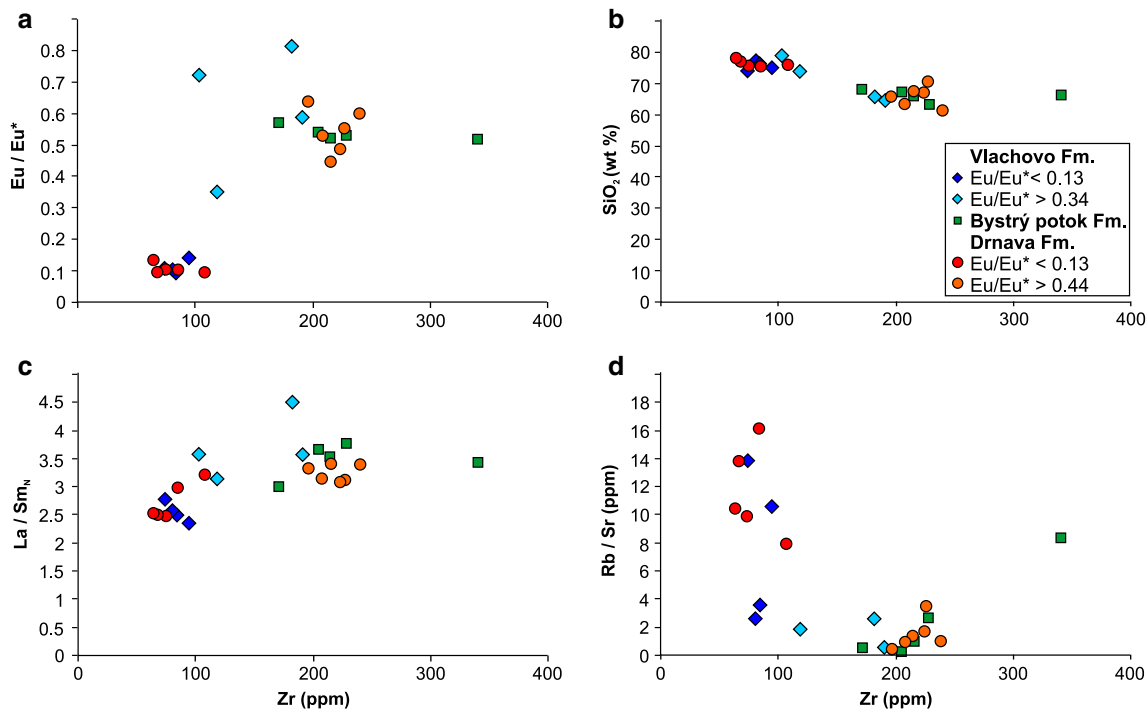


Fig. 4 Trace element discrimination diagrams of the studied metamavolcanic rocks: **a** Eu/Eu^* versus Zr, **b** SiO_2/Zr , **c** La/Sm_N versus Zr, **d** Rb/Sr versus Zr, sample GZ-4 is excluded for anomalous low Sr content

ages, with the degree of discordance, D , ranging between 3 and -6% . The common lead content, $^{206}\text{Pb}_c$, is low, usually less than 0.1% of the measured ^{206}Pb . The concentration of U and Th is low to moderate, $159\text{--}665$ and $88\text{--}345$ ppm, respectively. The $^{232}\text{Th}/^{238}\text{U}$ ratios are moderate, varying between 0.21 and 0.47 , with the exception of the one Paleoproterozoic inherited grain (point 2-1; Table 3), with the high $^{232}\text{Th}/^{238}\text{U}$ ratio (1.22). All these ratio values are characteristic for the crystallization within expected igneous conditions. The oldest data, $^{207}\text{Pb}/^{206}\text{Pb}$ 1945 ± 9 Ma, were obtained from the inherited grain that was enfolded by the newly formed oscillation zoned zircon of the 477 ± 7 Ma old (point 2-2; Table 3). The age data from the remaining eight grains, together with the rim of the inherited core, are scattered in the scale between 496 ± 7 and 477 ± 7 Ma. These set of analyses have been made from both, core as well as rim domains and gave the concordia age of 483 ± 5 Ma, corresponding with the Tremadocian (Fig. 9).

In the sample GZ-38, located WSW from the Gelnica town (Table 1), ten analyses from eight grains have been obtained (Table 3; Fig. 10a, b). The Precambrian inherited cores, $^{207}\text{Pb}/^{206}\text{Pb}$ 2606 ± 10 Ma (point 4-2) and $^{207}\text{Pb}/^{206}\text{Pb}$ 1961 ± 31 Ma (point 3-1), were enveloped by the newly formed magmatic zircons, 463 ± 10 Ma (point 3-2) and 438.5 ± 10 Ma (point 4-1). The calculated discordia (Fig. 10b) gave the upper intercepts at 2169 ± 81 (point

3-1) and 2647 ± 24 Ma (point 4-2), with the lower intercepts at 464 ± 27 Ma (point 3-2) and 435 ± 26 Ma (point 4-1). The remaining eight zircon ages varied from 486 to 457 Ma in both their rims and central part of crystals. These analytical spots gave the concordia age at 464 ± 7.5 Ma, with the moderate $^{235}\text{Th}/^{238}\text{U}$ ratios, mostly between 0.35 and 0.79 (Table 3; Fig. 10a). They have the variable U and Th concentrations, $156\text{--}490$ ppm and $92\text{--}718$ ppm, respectively.

Ten analytical points have been acquired from the rim of the ten grains in the sample of GZ-14, located NW from the Rákoš village (Table 1). All of these points yielded concordant or slightly discordant ages, with the degree of discordance, ranging between 10 and -10% . The U and Th contents are variable, $155\text{--}1113$ and $52\text{--}230$ ppm, respectively. The $^{232}\text{Th}/^{238}\text{U}$ ratios are mostly between 0.19 and 0.35 , typical for zircons of a magmatic origin. Some of the zircon grains from the sample GZ-14 seem to be incorporated from the older volcanogenic events. This is documented by three grains of the Cambrian age: 529 ± 7 , 516 ± 7 and 498 ± 7 Ma. The analytical points from the remaining six grains show the concordia age 461 ± 5 Ma (Fig. 11).

The zircon time span from the sample GZ-13 (Table 1) is bracketed within the wider range comparing with the samples GZ-14 and GZ-38. All the analytical points were positioned at the rims of the analysed zircon grains. Among

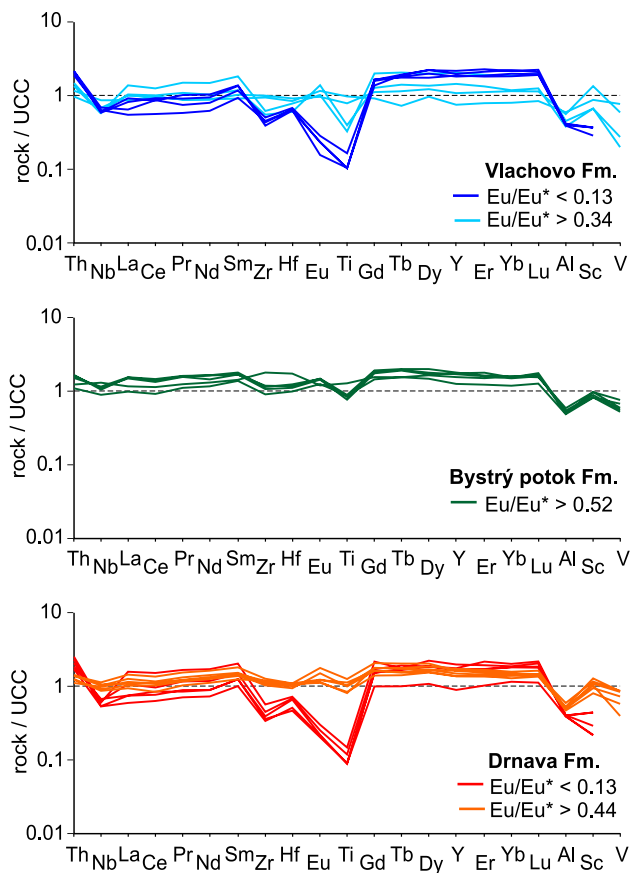


Fig. 5 Upper continental crust normalized incompatible elements distributions of the analysed samples (after Taylor and McLennan revised by McLennan 2001)

them, only five analytical points gave a relatively narrow time span, ranging between 448 and 471 Ma. The concordia age from these zircons corresponds with the age of 461 ± 6 Ma (Fig. 12) and with the $^{232}\text{Th}/^{238}\text{U}$ ratios between 0.08 and 0.37. The U and Th contents are highly variable, 175–1026 ppm and 23–136 ppm, respectively. The Cambrian ages, 491 ± 7 and 494 ± 7 Ma (Furongian), have been acquired from the other two grains. These ages document the process of zircon incorporation from the older volcanic events. The remaining three analytical points, yielded the following Proterozoic ages: $^{207}\text{Pb}/^{206}\text{Pb}$ 1971 ± 14 Ma, and $^{206}\text{Pb}/^{238}\text{U}$ ages of 620 ± 9 and 956 ± 13 Ma. All these analytical points were located at the rims of the individual crystals, as they are not inherited grains within the younger magmatic zircons (Fig. 7d). They represent recycled old crustal components. The sample *GZ-13* corresponds texturally with pyroclastic rocks and the admixture of detrital zircons is not excluded.

Discussion

Magma source and petrogenesis

The characteristic feature of the GG metavolcanic rocks is Rb, Th enrichment, together with LREE, and Nb–Ta depletion that is typical for volcanic arc magmatism related to ACM (Gorton and Schandl 2000; Pearce 1983, 1996b; Jenner et al. 1991; Arculus and Powell 1986; Brown et al. 1984; Wood et al. 1979). The

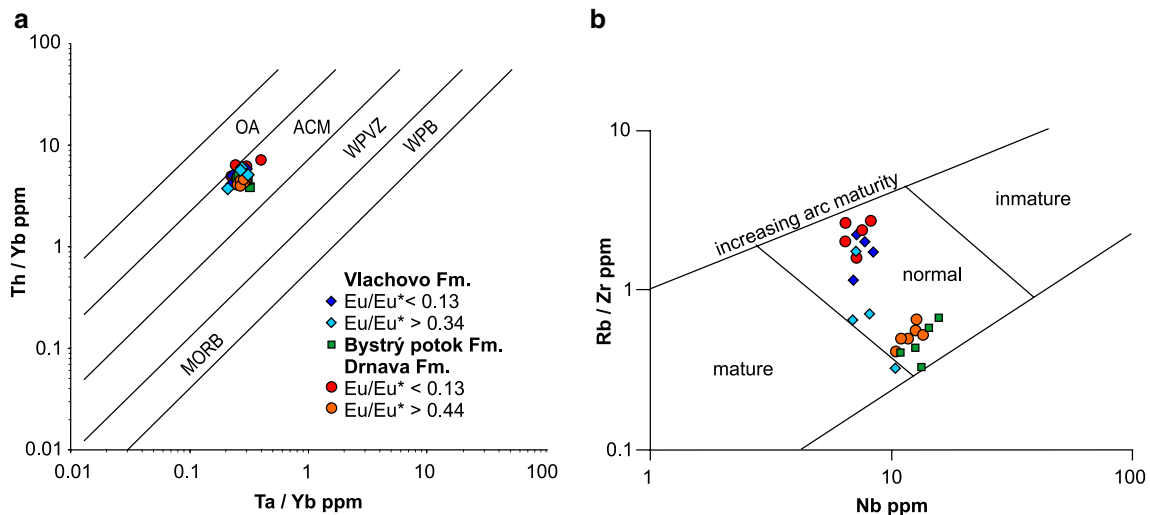


Fig. 6 Trace element discrimination diagrams for the tectonic interpretation of the SGU metavolcanic rocks. **a** Ta/Yb versus Th/Yb discrimination diagram after Gorton and Shandl (2000) (revised after Pearce 1983), **b** Rb/Sr versus Nb after Brown et al. (1984)



Fig. 7 CL zircon images from the SGU basement metavolcanic rocks: **a** sample GZ-15, **b** sample GZ-14, **c** sample GZ-38, **d** sample GZ-13, **e** sample GZ-37

chondrite-normalized patterns are also related for the GG metavolcanic rocks with different degree of fractionation (Fig. 3a). The most differentiated rocks show a slight increase of $(La/Yb)_N$ to the non-differentiated rocks, from 2.27 to 11.6, at a little variable $(Sm/Yb)_N$ ratios (from

1.6 for fractionated to 2.3 for non-fractionated magma, respectively). Similarly, these also display a distinct Eu trough (Eu/Eu^* 0.9–0.14), which instead is lacking the less differentiated rocks (Eu/Eu^* 0.35–0.81). The spider diagram of trace elements normalized to primitive mantle

Table 3 U–Pb (SHRIMP) magmatic zircon data from the Cambrian–Ordovician metavolcanic rocks

| Spot | ²⁰⁶ Pb _c % | U ppm | Th ppm | ²³² Th/ ²³⁸ U | ²⁰⁶ Pb* ppm | (1) ²⁰⁶ Pb/ ²³⁸ U age | ± | (1) ²⁰⁷ Pb/ ²⁰⁶ Pb age | ± | (1) ²⁰⁷ Pb* ²⁰⁶ Pb* | % | ± | (1) ²⁰⁷ Pb* ²³⁵ U | % | ± | (1) ²⁰⁶ Pb* ²³⁸ U | % | Err corr | |
|-------------------------|-------------------------------------|----------|-----------|--|---------------------------|--|-----|---|-----|---|-------|-----|---|------|-------|---|--------|----------|-------|
| <i>Bystřý potok Fm.</i> | | | | | | | | | | | | | | | | | | | |
| GZ-15.1 | 0.13 | 296 | 31 | 0.11 | 21.1 | 512.7 | 7.2 | 548 | 50 | 7 | 12.08 | 1.5 | 0.0585 | 2.3 | 0.667 | 2.7 | 0.0828 | 1.5 | 0.536 |
| GZ-15.2 | 0.05 | 658 | 29 | 0.05 | 43.6 | 478.8 | 6.4 | 498 | 32 | 4 | 12.97 | 1.4 | 0.0571 | 1.5 | 0.608 | 2 | 0.0771 | 1.4 | 0.691 |
| GZ-15.3 | 0.14 | 505 | 44 | 0.09 | 32.9 | 470.6 | 6.7 | 429 | 44 | -9 | 13.2 | 1.5 | 0.0554 | 2.0 | 0.579 | 2.5 | 0.0757 | 1.5 | 0.598 |
| GZ-15.4 | 0.34 | 307 | 10 | 0.03 | 19.4 | 455.9 | 6.8 | 412 | 55 | -10 | 13.65 | 1.6 | 0.055 | 2.4 | 0.556 | 2.9 | 0.0733 | 1.6 | 0.537 |
| GZ-15.5 | 0.38 | 428 | 86 | 0.21 | 22.6 | 382.6 | 5.4 | 486 | 72 | 27 | 16.35 | 1.5 | 0.0569 | 3.3 | 0.479 | 3.6 | 0.0611 | 1.5 | 0.409 |
| GZ-15.6 | 0.46 | 125 | 40 | 0.33 | 7.88 | 453.4 | 7.3 | 479 | 99 | 6 | 13.72 | 1.7 | 0.0567 | 4.5 | 0.569 | 4.8 | 0.0729 | 1.7 | 0.347 |
| GZ-15.7 | 0.30 | 600 | 57 | 0.10 | 38.2 | 459 | 6.5 | 406 | 48 | -11 | 13.55 | 1.5 | 0.0549 | 2.1 | 0.558 | 2.6 | 0.0738 | 1.5 | 0.566 |
| GZ-15.8 | 0.08 | 333 | 163 | 0.51 | 51.0 | 1057 | 14 | 1099 | 24 | 4 | 5.61 | 1.5 | 0.0761 | 1.2 | 1.872 | 1.9 | 0.1782 | 1.5 | 0.782 |
| GZ-15.9 | 0.36 | 233 | 38 | 0.17 | 14.7 | 453.9 | 7.1 | 450 | 78 | -1 | 13.71 | 1.6 | 0.0559 | 3.5 | 0.563 | 3.9 | 0.0729 | 1.6 | 0.418 |
| GZ-15.10 | 0.17 | 427 | 100 | 0.24 | 35.5 | 595.3 | 8.0 | 578 | 41 | -3 | 10.34 | 1.4 | 0.0593 | 1.9 | 0.791 | 2.3 | 0.0967 | 1.4 | 0.600 |
| GZ-15.11 | 0.40 | 378 | 28 | 0.08 | 23.5 | 450 | 6.3 | 327 | 84 | -27 | 13.83 | 1.4 | 0.053 | 3.7 | 0.528 | 4.0 | 0.0723 | 1.4 | 0.364 |
| <i>Drnava Fm.</i> | | | | | | | | | | | | | | | | | | | |
| GZ-14.1 | 0.07 | 552 | 145 | 0.27 | 40.6 | 529 | 7.5 | 493 | 35 | -7 | 11.69 | 1.5 | 0.0570 | 1.6 | 0.673 | 2.2 | 0.0855 | 1.5 | 0.681 |
| GZ-14.2 | 0.00 | 155 | 52 | 0.35 | 9.95 | 463.7 | 6.9 | 422 | 50 | -9 | 13.41 | 1.5 | 0.0553 | 2.2 | 0.568 | 2.7 | 0.0746 | 1.5 | 0.565 |
| GZ-14.3 | 0.09 | 368 | 102 | 0.29 | 23.7 | 466.3 | 6.4 | 489 | 37 | 5 | 13.33 | 1.4 | 0.0569 | 1.7 | 0.589 | 2.2 | 0.075 | 1.4 | 0.647 |
| GZ-14.4 | 0.28 | 287 | 103 | 0.37 | 20.6 | 516.1 | 7.3 | 463 | 66 | -10 | 12 | 1.5 | 0.0563 | 3.0 | 0.647 | 3.3 | 0.0834 | 1.5 | 0.443 |
| GZ-14.5 | 0.11 | 754 | 172 | 0.24 | 50.9 | 487 | 6.6 | 446 | 36 | -9 | 12.74 | 1.4 | 0.0558 | 1.6 | 0.604 | 2.2 | 0.0785 | 1.4 | 0.652 |
| GZ-14.6 | 0.16 | 1113 | 230 | 0.21 | 69.5 | 451.7 | 6.0 | 464 | 36 | 3 | 13.78 | 1.4 | 0.0562 | 1.6 | 0.563 | 2.1 | 0.0726 | 1.4 | 0.644 |
| GZ-14.7 | 0.33 | 388 | 117 | 0.31 | 24.6 | 457.8 | 6.5 | 462 | 56 | 1 | 13.59 | 1.5 | 0.0562 | 2.5 | 0.571 | 2.9 | 0.0736 | 1.5 | 0.504 |
| GZ-14.8 | 0.00 | 733 | 154 | 0.22 | 50.6 | 498.3 | 6.7 | 452 | 28 | -9 | 12.44 | 1.4 | 0.0559 | 1.3 | 0.62 | 1.9 | 0.0804 | 1.4 | 0.741 |
| GZ-14.9 | 0.06 | 663 | 124 | 0.19 | 42.3 | 461.5 | 6.3 | 443 | 32 | -4 | 13.47 | 1.4 | 0.0557 | 1.5 | 0.571 | 2.0 | 0.0742 | 1.4 | 0.695 |
| GZ-14.10 | 0.35 | 574 | 128 | 0.23 | 37.0 | 464.3 | 6.4 | 509 | 48 | 10 | 13.39 | 1.4 | 0.0575 | 2.2 | 0.592 | 2.6 | 0.0747 | 1.4 | 0.546 |
| GZ-13.1 | 0.12 | 505 | 44 | 0.09 | 34.4 | 491.2 | 7.0 | 460 | 41 | -6 | 12.63 | 1.5 | 0.0562 | 1.8 | 0.614 | 2.4 | 0.0792 | 1.5 | 0.625 |
| GZ-13.2 | 0.24 | 384 | 136 | 0.37 | 24.8 | 466.2 | 6.9 | 414 | 72 | -11 | 13.33 | 1.5 | 0.055 | 3.2 | 0.569 | 3.6 | 0.075 | 1.5 | 0.427 |
| GZ-13.3 | 0.11 | 326 | 35 | 0.11 | 20.2 | 448.1 | 6.8 | 445 | 80 | -1 | 13.89 | 1.6 | 0.0558 | 3.6 | 0.554 | 3.9 | 0.072 | 1.6 | 0.402 |
| GZ-13.4 | 0.07 | 365 | 88 | 0.25 | 50.2 | 956 | 13 | 961 | 29 | 1 | 6.254 | 1.4 | 0.0711 | 1.4 | 1.568 | 2.0 | 0.1599 | 1.4 | 0.706 |
| GZ-13.5 | 0.13 | 339 | 52 | 0.16 | 23.2 | 493.9 | 7.1 | 475 | 52 | -4 | 12.56 | 1.5 | 0.0566 | 2.4 | 0.621 | 2.8 | 0.0796 | 1.5 | 0.534 |
| GZ-13.6 | 0.65 | 216 | 239 | 1.14 | 18.8 | 619.6 | 9.0 | 555 | 94 | -10 | 9.91 | 1.5 | 0.0587 | 4.3 | 0.816 | 4.6 | 0.1009 | 1.5 | 0.335 |
| GZ-13.7 | 0.97 | 1026 | 76 | 0.08 | 67.6 | 471.6 | 6.4 | 402 | 60 | -15 | 13.17 | 1.4 | 0.0548 | 2.7 | 0.573 | 3.0 | 0.0759 | 1.4 | 0.465 |
| GZ-13.8 | 0.03 | 302 | 97 | 0.33 | 72.0 | 1578 | 20 | 1971 | 14 | 25 | 3.605 | 1.4 | 0.121 | 0.81 | 4.628 | 1.6 | 0.2774 | 1.4 | 0.867 |
| GZ-13.9 | 0.42 | 369 | 43 | 0.12 | 23.5 | 458 | 6.5 | 418 | 79 | -9 | 13.58 | 1.5 | 0.0551 | 3.5 | 0.56 | 3.8 | 0.0736 | 1.5 | 0.386 |
| GZ-13.10 | 0.30 | 175 | 23 | 0.14 | 11.2 | 462.3 | 7.3 | 470 | 110 | 2 | 13.45 | 1.6 | 0.0564 | 5.1 | 0.579 | 5.3 | 0.0743 | 1.6 | 0.307 |

Table 3 continued

| Spot | $^{206}\text{Pb}_c$ % | U ppm | Th ppm | $\frac{^{232}\text{Th}}{^{238}\text{U}}$ | $^{206}\text{Pb}^*$ ppm | (1) $\frac{^{206}\text{Pb}}{^{238}\text{U}}$ age | \pm | (1) $\frac{^{207}\text{Pb}}{^{206}\text{Pb}}$ age | \pm | Discordant % | (1) $\frac{^{238}\text{U}}{^{206}\text{Pb}^*}$ | \pm % | (1) $\frac{^{207}\text{Pb}^*}{^{206}\text{Pb}^*}$ | \pm % | (1) $\frac{^{207}\text{Pb}^*}{^{235}\text{U}}$ | \pm % | (1) $\frac{^{206}\text{Pb}^*}{^{238}\text{U}}$ | \pm % | Err corr |
|---------------------|--------------------------|----------|-----------|--|----------------------------|--|-------|---|-------|-----------------|---|------------|--|------------|---|------------|---|------------|----------|
| GZ-38.1 | 0.06 | 216 | 92 | 0.44 | 13.9 | 464 | 11 | 485 | 67 | 4 | 13.39 | 2.4 | 0.0568 | 3.0 | 0.585 | 3.8 | 0.0747 | 2.4 | 0.619 |
| GZ-38.2 | 0.03 | 243 | 139 | 0.59 | 16.4 | 486 | 11 | 521 | 47 | 7 | 12.78 | 2.4 | 0.0578 | 2.2 | 0.623 | 3.2 | 0.0783 | 2.4 | 0.739 |
| GZ-38.3-1 | 0.18 | 221 | 44 | 0.20 | 41.6 | 1273 | 26 | 1961 | 31 | 54 | 4.58 | 2.3 | 0.1203 | 1.7 | 3.62 | 2.9 | 0.2183 | 2.3 | 0.796 |
| GZ-38.3-2 | 0.06 | 490 | 186 | 0.39 | 31.4 | 463 | 10 | 458 | 59 | -1 | 13.42 | 2.3 | 0.0561 | 2.6 | 0.577 | 3.5 | 0.0745 | 2.3 | 0.650 |
| GZ-38.4-1 | 0.31 | 274 | 175 | 0.66 | 16.6 | 438.5 | 9.9 | 482 | 94 | 10 | 14.21 | 2.3 | 0.0567 | 4.2 | 0.551 | 4.8 | 0.0704 | 2.3 | 0.481 |
| GZ-38.4-2 | - | 300 | 285 | 0.98 | 107 | 2237 | 43 | 2605.7 | 10 | 16 | 2.411 | 2.3 | 0.175 | 0.6 | 10.01 | 2.3 | 0.4148 | 2.3 | 0.966 |
| GZ-38.5 | 0.28 | 156 | 69 | 0.46 | 10.3 | 475 | 11 | 348 | 100 | -27 | 13.07 | 2.4 | 0.0534 | 4.5 | 0.564 | 5.1 | 0.0765 | 2.4 | 0.473 |
| GZ-38.6 | 0.21 | 934 | 718 | 0.79 | 59.0 | 456.5 | 9.8 | 508 | 71 | 11 | 13.63 | 2.2 | 0.0574 | 3.2 | 0.581 | 3.9 | 0.0734 | 2.2 | 0.570 |
| GZ-38.7 | 0.06 | 299 | 101 | 0.35 | 19.4 | 468 | 10 | 434 | 48 | -7 | 13.27 | 2.3 | 0.0555 | 2.2 | 0.577 | 3.2 | 0.0754 | 2.3 | 0.727 |
| GZ-38.8 | 0.06 | 300 | 129 | 0.45 | 19.3 | 467 | 14 | 507 | 47 | 9 | 13.32 | 3.1 | 0.0574 | 2.1 | 0.594 | 3.8 | 0.0751 | 3.1 | 0.827 |
| <i>Vlachovo Fm.</i> | | | | | | | | | | | | | | | | | | | |
| GZ-37.1 | 0.03 | 376 | 105 | 0.29 | 24.9 | 478.4 | 7.0 | 491 | 27 | 3 | 12.98 | 1.5 | 0.05699 | 1.2 | 0.605 | 1.9 | 0.077 | 1.5 | 0.781 |
| GZ-37.2-1 | 0.02 | 292 | 345 | 1.22 | 88.7 | 1948 | 25 | 1945.3 | 8.6 | 0 | 2.834 | 1.5 | 0.11927 | 0.48 | 5.801 | 1.6 | 0.3528 | 1.5 | 0.952 |
| GZ-37.2-2 | 0.14 | 294 | 98 | 0.34 | 19.4 | 477 | 7.0 | 470 | 41 | -2 | 13.02 | 1.5 | 0.0564 | 1.8 | 0.598 | 2.4 | 0.0768 | 1.5 | 0.639 |
| GZ-37.3 | 0.07 | 402 | 88 | 0.22 | 26.8 | 480.3 | 7.0 | 498 | 27 | 4 | 12.93 | 1.5 | 0.05718 | 1.2 | 0.61 | 2.0 | 0.0773 | 1.5 | 0.776 |
| GZ-37.4 | 0.00 | 573 | 258 | 0.47 | 38.2 | 481.6 | 7.1 | 478 | 26 | -1 | 12.89 | 1.5 | 0.05665 | 1.2 | 0.606 | 1.9 | 0.0776 | 1.5 | 0.788 |
| GZ-37.5 | 0.02 | 665 | 186 | 0.29 | 44.3 | 480.8 | 6.9 | 466 | 20 | -3 | 12.91 | 1.5 | 0.05635 | 0.92 | 0.602 | 1.8 | 0.0774 | 1.5 | 0.852 |
| GZ-37.6 | 0.00 | 279 | 84 | 0.31 | 18.8 | 487.1 | 7.2 | 456 | 30 | -6 | 12.74 | 1.5 | 0.0561 | 1.3 | 0.607 | 2.0 | 0.0785 | 1.5 | 0.754 |
| GZ-37.7 | 0.00 | 642 | 201 | 0.32 | 44.2 | 496.3 | 7.1 | 479 | 35 | -3 | 12.5 | 1.5 | 0.05669 | 1.6 | 0.626 | 2.2 | 0.08 | 1.5 | 0.681 |
| GZ-37.8 | 0.09 | 159 | 33 | 0.21 | 10.7 | 486.3 | 7.5 | 469 | 45 | -3 | 12.76 | 1.6 | 0.0564 | 2.1 | 0.61 | 2.6 | 0.0783 | 1.6 | 0.616 |
| GZ-37.9 | 0.06 | 335 | 90 | 0.28 | 22.2 | 479.5 | 7.1 | 475 | 29 | -1 | 12.95 | 1.5 | 0.05658 | 1.3 | 0.602 | 2.0 | 0.0772 | 1.5 | 0.758 |

Errors are 1 sigma; Pb_c and Pb^* indicate the common and radiogenic portion, respectively. Error in Standard calibration was 0.51% for GZ-37; 0.73% for GZ-38 and 0.53% for GZ-13, 14, 15 (not included in above errors but required when comparing data from different mounts). (1) Common Pb corrected using measured ^{204}Pb

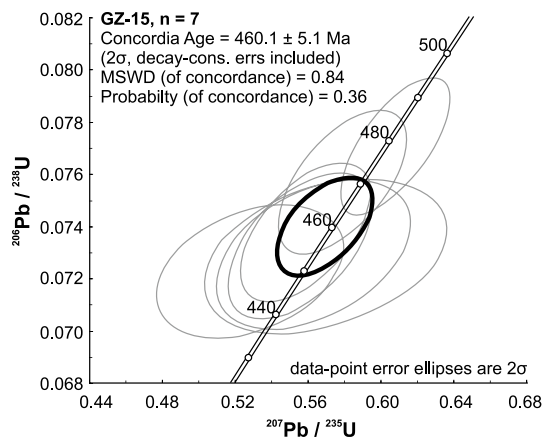


Fig. 8 Concordia diagrams of dated magmatic zircons from the sample GZ-15: zircon age data based on the $^{206}\text{Pb}/^{238}\text{U}$ versus $^{207}\text{Pb}/^{235}\text{U}$ ratios

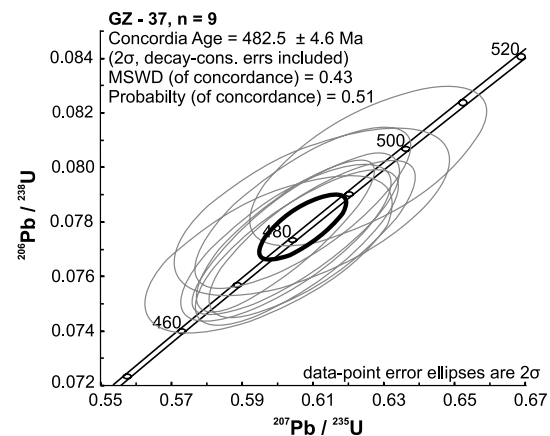


Fig. 9 Concordia diagrams of dated magmatic zircons from the sample GZ-37: zircon age data based on the $^{206}\text{Pb}/^{238}\text{U}$ versus $^{207}\text{Pb}/^{235}\text{U}$ ratios

(Fig. 3b) shows depletion of HFSE (manifested troughs at Nb and Ti) with respect to LILE and LREE, as it is representative for arc magma. The whole set of sample shares very similar patterns, with a general enrichment of Rb, Th and LREE towards the most differentiated metavolcanic rocks. Their UCC-normalized patterns are relatively flat (Fig. 5), with depletion in Nb, Ti, Sc, V and enrichment in Th. Depletions in Ti, V, and to the lesser extent Nb, are consistent with oxide fractionation at high levels in the crust (Piercey et al. 2006). Generally, all the SGU metavolcanic rocks have a low Nb and Y values (Table 2), characteristic for volcanic arc magmatites. Nevertheless, the $(\text{La}/\text{Sm})_{\text{UCN}}$ ratios in the SGU metavolcanites are systematically depleted relative to UCC, with $(\text{La}/\text{Sm})_{\text{UCN}} < 1$. This process required either depleted source, for example mafic crust or the fractionation of LREE-bearing accessory phases. In detail, the fractionated GG metavolcanic rocks are more depleted in LREE than non-fractionated ones. Thus, the process fractionating of LREE-bearing phase is more likely. Consequently, the majority of REE fractionation can be explained by feldspar, hornblende, zircon, monazite and apatite crystallization. All these minerals are among the observed phenocryst assemblages. Similarly, the Zr versus Eu/Eu^* and Rb/Sr ratios, as well as SiO_2 versus Zr ratios (Fig. 4a, b, d), imply that the SGU metavolcanites have undergone an extensive magmatic fractionation.

Both group of the studied metavolcanites, silicic and intermediate, have low HFSE contents (Zr, Nb, Y, Ti, Hf, Ta) and low to intermediate Zr/Sc (22.5–13.2 and 26.2–10.6, respectively) and Zr/TiO₂ (1208–540 and 268–405, respectively) ratios, when compared with non-arc and A-type felsic rocks (for comparing Piercey et al. 2006 and references therein). A crystal fractionation signature in the SGU acid metavolcanites is indicated by the higher Rb/Sr

ratios (1.32–16.1) comparing with the co-genetic intermediate members (0.22–3.40).

According to Bachmann and Bergantz (2004, 2008), a spatial and chronological proximity between crystal-poor rhyolites and crystal-rich intermediate magma supports the idea of interstitial extraction from batholithic crystal mushes, with a typical partitioning coefficients for Rb and Sr. Melt expulsion from the crystal mush predicts the extended age range recorded by zircons in silicic magmas (Brown and Fletcher 1999). In fact, in the SGU acid, metavolcanites were also zircon grains that might have had a longer crystallization period, indicating a scattering of analytical data.

As pointed out by Christiansen (2005) and Christiansen and McCurry (2008), rhyolites can be divided into two categories: (1) the hot-dry-reduced that occurred mostly in mantle-upwelling and continental rifts areas; (2) the cold-wet-oxidized, typically found in subduction zones. Both type of rhyolites show different trace element contents, in particular for REE. In wet-oxidizing environment, crystallization of amphibole and titanite, which sequester middle REE and heavy REE (Glazner et al. 2008; Bachmann et al. 2005 and references therein), produces REE patterns with smaller Eu-negative anomalies. The SGU intermediate Cambrian–Ordovician metavolcanites have depletion in the middle and heavy REE and smaller Eu-negative anomalies, characteristic for cold-wet-oxidizing subduction-related volcanics. In the highly evolved SGU metavolcanites (>70 wt% SiO₂), the REE patterns show deep Eu negative anomalies even at equal or nearly similar concentrations of middle and heavy REE comparing to the intermediate members (Fig. 3a). Plagioclases crystallization that removes Eu from the melt plays the major role for these deep Eu negative anomalies. According to Bachmann and Bengratz (2004, 2008 and references therein), these deep Eu anomalies are more typical for drier magmas, resulting

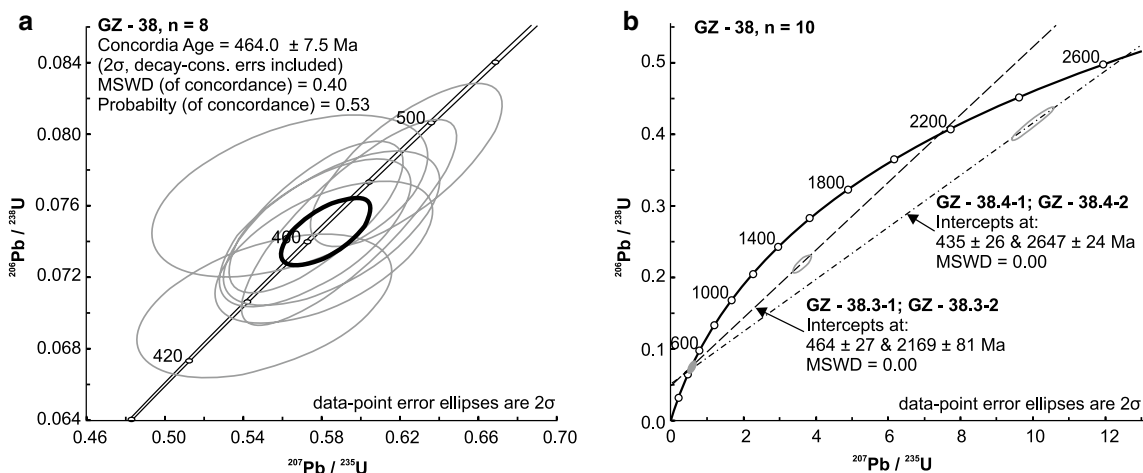


Fig. 10 Concordia diagrams of dated magmatic zircons from the sample GZ-38: **a** zircon age data based on the $^{206}\text{Pb}/^{238}\text{U}$ versus $^{207}\text{Pb}/^{235}\text{U}$ ratios, **b** calculated discordia intercepts for the inherited grains from the sample GZ-38

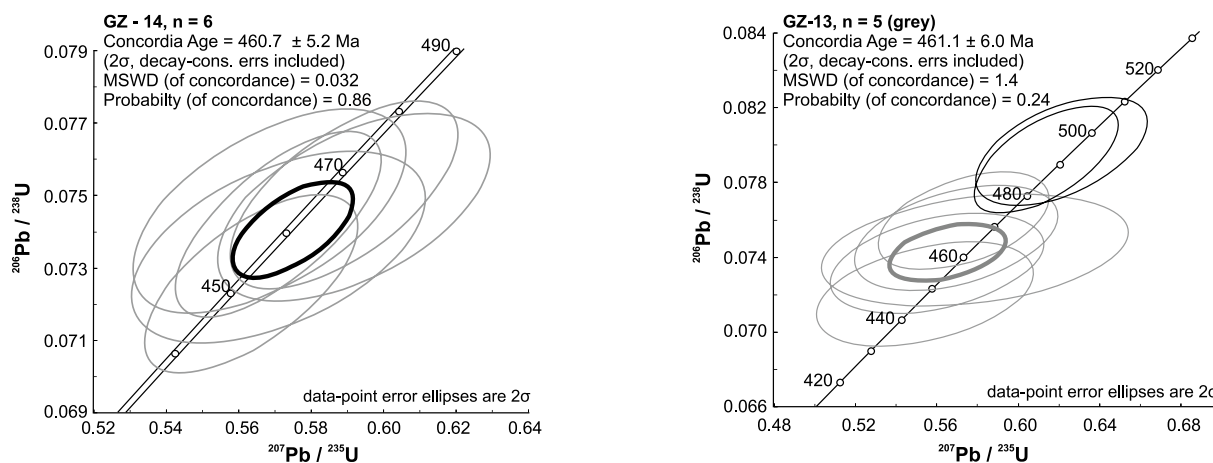


Fig. 11 Concordia diagrams of dated magmatic zircons from the sample GZ-14: zircon age data based on the $^{206}\text{Pb}/^{238}\text{U}$ versus $^{207}\text{Pb}/^{235}\text{U}$ ratios

Fig. 12 Concordia diagrams of dated magmatic zircons from the sample GZ-13 (grey circle—samples used for average age calculation): zircon age data based on the $^{206}\text{Pb}/^{238}\text{U}$ versus $^{207}\text{Pb}/^{235}\text{U}$ ratios

from a hot and extensional tectonic setting. However, the SGU acid metavolcanics are thus in discrepancy to this with the diminishing of the middle and heavy REE.

The SGU metavolcanics display the geochemical trends that suggest a petrogenetic history involving significant fractional crystallization process in producing high-SiO₂ magmas. The crustal assimilation is supported by the Proterozoic–Archaean xenocrystic grains in the magmatic zircons cores.

Zircon dating

In the four analysed samples, collected from the BPF (sample GZ-15) and DF formations (samples GZ-38, GZ-14 and GZ-13), majority of zircon analyses yielded the consistent

concordia ages, ranging between 464 and 460 Ma (Figs. 9, 10a, 11, 12). These correspond with the uppermost Middle Ordovician, at the Darriwilian stage (after ICS Chronostratigraphic Chart 2016). The detected zircon ages clearly confirm the previous zircon dating (Vozárová et al. 2010). The metavolcanites from the both lithostratigraphic units belong to the consistent volcanic event, with the DF and BPF concordia ages of 464 and 466 Ma, respectively. The quoted $^{206}\text{Pb}/^{238}\text{U}$ ages are concordant and thus provide the unbiased estimates for the zircon growth ages, originating during the magma crystallization. The five Cambrian grains in the time span of 529–491 Ma could be a product of a reworking and recycling from the earlier magmatic events and have been incorporated during ascent and emplacement of the youngest, Darriwilian magma at ~464 Ma.

The sample *GZ-37*, collected from the DF (based of Bajaník et al. 1983 lithostratigraphic classification), shows the concordia age of 483 Ma (Fig. 8). This is, comparing with the previous four samples a surprising result, since the *GZ-37* zircon assemblage is more than 20 Ma older. This age is fully consistent with the zircon ages from the upper part of the VF, lowermost lithostratigraphic unit of the Gelnica Group (485 and 481 Ma; Vozárová et al. 2010). Considering this, it would be necessary to correct the NE limit of the DF and re-define the NE part of DF and keep it as the lithostratigraphic part that belongs to the VF (Fig. 1). The 482 Ma zircon age published by Putiš et al. (2008) fits well this conception.

Thus, fifteen SHRIMP zircon ages (present zircon ages together with data taken from Vozárová et al. 2010) from the Southern Gemicum basement document the Early Palaeozoic poly-magmatic events. Based on the first results of zircon dating, two major magmatic phases were recognized (Vozárová et al. 2010), which correspond with distinct periods of magmatic zircon growth. First, in Late Cambrian/Early Ordovician and the second, in Middle Ordovician times. The presented new set of zircon dating confirms, generally, these magmatic sequences. However, new zircon data enable us to separate the first magmatic phase into the Late Cambrian and Early Ordovician, at ca. 492 and 481 Ma, respectively, with 11 Ma gap between them (Fig. 13a, b). As the consequence, three magmatic phases could be recognized within the Early Palaeozoic basement of the Southern Gemicum. They correspond with the early-mid Furongian (peak at 492 Ma), Tremadocian (peak at 481 Ma) and Darriwilian (peak at 464 Ma) times (Fig. 13b). The Darriwilian magmatic phase offered the youngest concordia zircon age at 447 ± 7 Ma (sample *GZ-7* in Vozárová et al. 2010) in the central part of the BPF occurrences (Fig. 1). This is reflected in the BPF probability density plot (Fig. 13b) with the maximum peak at 453 Ma, which straddle the boundary between Sandbian and Katian of the Upper Ordovician (after ICS Stratigraphic Chart 2016). This is considered as the evidence that Darriwilian magmatic phase terminated in the early Upper Ordovician. The presence of the youngest detrital zircons in the BPF sandstones and their age (Vozárová et al. 2012) that is overlapping with the youngest magmatic zircon population, documents the presumed closing of the supposed fore-arc GG sedimentary basin (Fig. 13b).

U–Pb zircon isotopic data support the idea that the SGU Cambrian–Ordovician magmatic arc involved juvenile magmas that were contaminated with varying amount of Cadomian, Tonian–Stenian and Eburnian crust. According to this, the Cambrium–Ordovician magmatic arc and appropriated fore-arc basin should be situated at NE part of Gondwanan margin along the Saharan Metacraton.

Provenance implications

Zircon xenocrystic grains in these metavolcanic rocks clearly indicate remelting and recycling of older crustal components. The U–Pb zircon ages from xenocrystic grains commonly identify a Proterozoic and Archaean inheritance (present data and Vozárová et al. 2010). These zircon populations (42 spots together) are dominated by Ediacarian–Cryogenian (~550–800 Ma; 19 spots, ca. 46%) xenocrystic zircon grains, with less frequent of Tonian–Stenian (~0.9–1.1 Ga; 4 spots, ca 9%), Mesoproterozoic (~1.3–1.5 Ga; 5 spots, ca 12%), Paleoproterozoic (~1.9–2.4 Ga; 19 spots, ca 19%) and Archaean grains (~2.6–2.8 Ga and single zircons of 3.2 Ga; 6 spots, ca 14%) (Fig. 13a). Relevant detrital zircon assemblages (47 grains), obtained from the associated metasediments of the all three GG lithostratigraphic units, consist of the identical zircon populations. There is dominant Ediacarian–Cryogenian 550–800 Ma zircon population (23 spots, ~49%), with varying percentage of the Tonian–Stenian 0.9–1.1 Ga (9 spots, ~19%), Mesoproterozoic 1.3–1.4 Ga (1 spot, ~2%), Paleoproterozoic 1.7–2.4 Ga (8 spots, ~17%) and Archaean 2.8–2.6 Ga (6 spots, ~13%) populations (Fig. 13a). The youngest detrital zircon of 452 ± 8 Ma (2 grains) overlaps the age maximum of the GG deposition (Fig. 13b) in the middle-late Ordovician (data from Vozárová et al. 2012). Most of these detrital zircons yielded concordant Neoproterozoic ages, indicating that the GG metasandstones consist mainly of peri-Gondwanan Avalonian–Cadomian arc erosional detritus, which was active between ~750 and 550 Ma (Linnemann et al. 2014; Murphy et al. 2013; Nance et al. 2008; Nance and Murphy 1994; Murphy and Nance 1989). The obtained zircons populations were previously attributed to the Avalonian–Amazonian provenance (Vozárová et al. 2010, 2012), referred to as the continental reconstruction in the late Neoproterozoic-early Palaeozoic that placed Avalonia along the Amazonian margin of Gondwana (Nance et al. 2008; Scotese 2004; Stampfli and Borel 2002). The acquired zircon data indicate a period of mixing between juvenile and Paleoproterozoic crust (2.2–2.4 Ga) at ~900–1050 Ma typical for Amazonia. On the other hand, the interval of zircon generation of ~0.8–0.9 Ga, associated with Amazonian Goiás magmatic arc (0.6–0.9 Ga), developed during the Tonian–Ediacaran (Pimentel et al. 2011; Cordani et al. 2009), was not found in the GG zircon populations, similarly as in the Neoproterozoic assemblages of Avalonia (Thompson et al. 2012). Early Neoproterozoic gap is not characteristic for the Amazonia sources. However, the distinct magmatic gap between 0.8–0.9 Ga was documented in Baltica by U–Pb–Hf isotopic study, related to the Timanides orogeny (Kuznetsov et al. 2010). This was a crucial argument for the Henderson's et al. (2015) and Thompson's et al. (2012) interpretation that Avalonia was located near

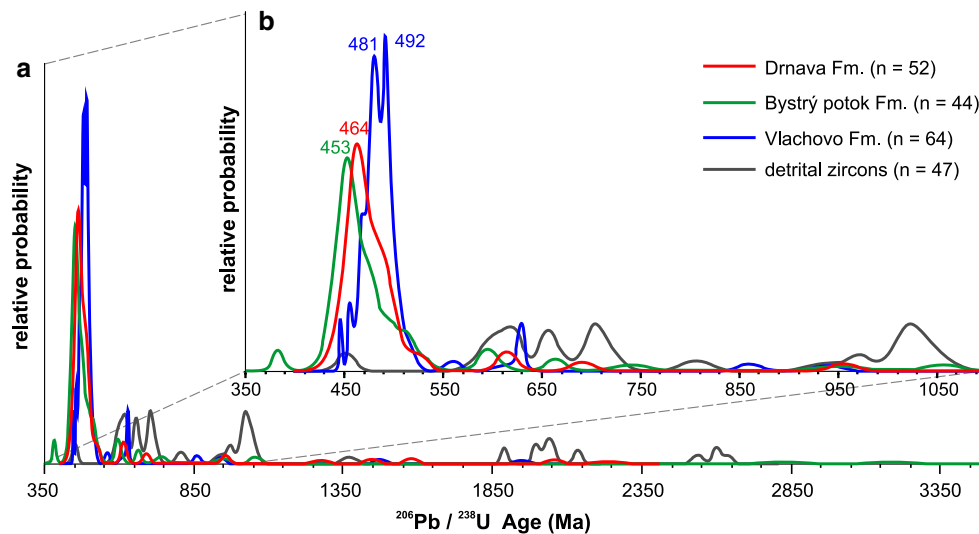


Fig. 13 Relative probability plots of the magmatic and detrital $^{206}\text{Pb}/^{238}\text{U}$ zircon age data from the SGU early Palaeozoic basement: **a** age time span from 0.35 to 3.5 Ga, **b** age time span from 0.35 to

1.1 Ga. Data for metavolcanic zircons are from the present paper and taken from Vozárová et al. (2010) and data for detrital zircons from non-volcanic metasediments are taken from (Vozárová et al. 2012)

Baltica and not near Amazonia in the early Neoproterozoic time.

Further, there are some differences between Avalonian zircon populations and those obtained from the GG detrital populations as well as from inherited zircons of the Cambrian–Ordovician metavolcanic rocks. There are: (1) the presence of Tonian–Stenian 0.9–1.1 Ga zircon population (9–19%) and (2) the expressionless Mesoproterozoic population spanned from 1.3 to 1.4 Ga (2–12%). First, the Tonian–Stenian zircon populations are missing in the Avalonian provenance and second, the Mesoproterozoic zircon populations are with a wider time span, from 1.2 to 1.6 Ga (Linnemann et al. 2012; Pimentel et al. 2011; Matteini et al. 2010; Cordani et al. 2009 and references therein). Between Paleoproterozoic and Archaean zircon populations (1.7–2.4 Ga and 2.6–3.2 Ga), no significant differences were found. The small peak at 2.0–2.1 Ga is characteristic for the Southern Gemicum GG rock sequence. Generally, these zircon populations reflect the global 1.8–2.1 Ga collisional orogenic events, referred to as the existence of pre-Rodinia supercontinent (Zhao et al. 2002; Rogers and Santosh 2002 and references therein). The cratonic blocks in South America and West Africa were welded by 2.0–2.1 Ga Transamazonian and Eburnian Orogeny (Henderson et al. 2015; Zhao et al. 2002). These zircon populations were described from several Archaean and Paleoproterozoic cratonic blocks, e.g. in the West African Craton (Linnemann et al. 2014; Abati et al. 2012; Walsh et al. 2012), Saharan Metacraton (Be’eri-Shlevin et al. 2014; Iizuka et al. 2013; Abdesalan et al. 2002) and Amazonia (Cordani and Teixeira 2007; Winchester et al. 2006; Nance and Murphy 1994). Such

a reworked zircon detritus is present in many terranes of the European and Alpine Variscides, e.g. the Central and NW Iberia (Fernández-Suárez et al. 2014, 2002; Talavera et al. 2013; Gutiérrez-Alonso et al. 2003), the Alpine basement of Switzerland and Austria (Neubauer et al. 2002; vonRaumer et al. 2013), the Serbo-Macedonian Massif in Greece (Meinhold et al. 2010), the Eastern and Southern Carpathians (Balintoni and Balica 2013 and references therein), the Western Carpathians (Vozárová et al. 2010, 2012) and the Istanbul terrane in NW Turkey (Ustaömer et al. 2011).

Our present zircon data, together with the reinterpretation of the previously published detrital and inherited zircon ages (Vozárová et al. 2012) clearly demonstrate the principal Neoproterozoic source, derived from the Peri-Gondwanan Avalonian–Cadmian arc, with the dominated Ediacaran 560–670 Ma zircon populations for the Southern Gemicum basement. Less frequent Tonian–Stenian 0.9–1.1 Ga, mid-Paleoproterozoic 1.8–2.4 Ga and Archaean 2.5–2.8 Ga zircon grains were incorporated into the juvenile Neoproterozoic crust from the reworked Paleo-Proterozoic–Archaean crustal fragments. The absence or insignificant amount of the Mesoproterozoic zircons (1 detrital zircon grain in metasediments and 5 xenocrystic grains in metavolcanic rocks) is a characteristic. The distribution of the Proterozoic–Archaean and Tonian–Stenian inherited and detrital zircons and deficiency of the Mesoproterozoic grains indicate more similarities with the Saharan Metacraton provenance than with the Amazonia Craton that was tentatively presupposed by Vozárová et al. (2012). This interpretation is compatible with the results and indications of Henderson et al. (2015).

Conclusions

The conclusions may be summarized as follows:

1. U–Pb SHRIMP magmatic zircon ages from the Southern Gemicum Unit proved the long-lived acid to intermediate continental magmatic arc volcanism with maximum activities in the mid-late Furongian (~492 Ma), Tremadocian (~481 Ma) and Darriwilian (~464 Ma). Darriwilian volcanic activity was prolonged into late Ordovician, with the peak activity at 453 Ma, at least within the Bystrý potok Formation. This is consistent with the closing of the GG sedimentary fore-arc basin, which is indicated by detrital zircon within the associated metasandstones, at 453 Ma.
2. The low (Nb + Y) content is the diagnostic feature for the Southern Gemicum metavolcanics that is characteristic for volcanic arc in subduction-related setting. Mantle-crust interaction together with process of a fractional crystallization produced an intermediate to acid magma.
3. Zircon xenocrystic grains in the Cambrian–Ordovician metavolcanics indicate a remelting and recycling of juvenile Avalonian–Cadomian crust, with the dominated Ediacaran 560–670 Ma zircon populations and significant older crustal components (Tonian–Stenian 0.9–1.1 Ga, mid-Paleoproterozoic 1.8–2.4 Ga and Archaean 2.6–2.8 Ga zircon grains). These acquired zircon age populations are consistent with the detrital zircon assemblages previously described from the associated metasandstones (Vozárová et al. 2012).
4. Dominance of the Ediacaran with lesser extent of Tonian–Stenian and Proterozoic–Archaean inherited and detrital zircons as well as the deficiency of Mesoproterozoic zircon grains point at similarities with the Saharan Metacraton provenance and location of the SGU Cambrian–Ordovician magmatic arc along NE Gondwanan margin.

Acknowledgements The financial support of the Slovak Research and Development Support Agency (Project ID: APVV-0546-11) is gratefully acknowledged. The authors would like to thank M. Kohút and L. Krmíček for constructive reviews which led to significant improvement of this manuscript.

References

- Abati J, Aghzler AM, Gerdes A, Ennih N (2012) Insights on the crustal evolution of the West African Craton from Hf isotopes in detrital zircons from Anti-Atlas belt. *Precambrian Res* 212–213:263–274
- Abdesalan MG, Liègeois JP, Stern RJ (2002) The Saharan metacraton. *J Afr Earth Sci* 34:119–136. doi:10.1016/S0899-5362(02)00013-1
- Abonyi A (1971) Stratigraphic and tectonic evolution of the Gemic Carboniferous at west from the Štútník Fault. *Geologické Práce Správy* 57:339–348 (in Slovak)
- Andrusov D (1968) Grundriss der Tektonik der Nördlichen Karpaten. Slovak Academy of Sciences, Bratislava, p 188
- Arculus RJ, Powell R (1986) Source component mixing in the regions of magma generation. *J Geophys Res* 91:5913–5926
- Bachmann O, Bergantz GW (2004) On the origin of crystal-poor rhyolites: extracted from batholithic crystal mushes. *J Petrol* 45(8):1565–1582. doi:10.1093/petrology/egh019
- Bachmann O, Bergantz GW (2008) Rhyolites and their source mushes across tectonic settings. *J Petrol* 49(12):2277–2285. doi:10.1093/petrology/egn068
- Bachmann O, Dungan MA, Bussy F (2005) Insights into shallow magmatic processes in large silicic magma bodies: the trace element record in the Fish Canyon magma body, Colorado. *Contrib Mineral Petrol* 149:338–349
- Bajaník Š, Hanzel V, Ivanička J, Mello J, Pristaš J, Reichwalder P, Snopko L, Vozár J, Vozárová A (1983) Explanation to geological map of the Slovenské rudohorie Mts.—eastern part. D Štúr Inst Geol Publ House, Bratislava, p 223 (in Slovak)
- Bajaník Š, Ivanička J, Mello J, Pristaš J, Reichwalder P, Snopko L, Vozár J, Vozárová A (1984) Geological map of the Slovenské rudohorie Mts.— eastern part, 1:50,000. D Štúr Inst Geol, Bratislava
- Balintoni I, Balica C (2013) Carpathian peri-Gondwanan terranes in the East Carpathians (Romania): a testimony of an Ordovician, North African orogeny. *Gondwana Res* 23:1053–1070
- Barrett TJ, MacLean WH (1994) Chemostratigraphy and hydrothermal alteration in exploration for VHMS deposits in greenstones and younger volcanic rocks. In: Lentz DR (ed) Alteration and alteration processes associated with ore-forming systems. Short course notes no 11. Geological Association of Canada, Toronto, Ontario, pp 433–467
- Be'eri-Shlevin Y, Avigad D, Gerdes A, Zlatkin O (2014) Detrital zircon U–Pb–Hf systematics of Israeli coastal sands: new perspectives on the provenance on Nile sediments. *J Geol Soc* 171(1):107–116
- Biely A, Bezák V, Elečko M, Gross P, Kaličiak M, Konečný V, Lexa J, Mello J, Nemčok J, Potfaj M, Rakús M, Vass D, Vozár J, Vozárová A (1996a) Explanation to geological map of Slovakia, 1:500,000. Dionýz Štúr Publisher, Bratislava, p 76
- Biely A, Bezák V, Elečko M, Gross P, Kaličiak M, Konečný V, Lexa J, Mello J, Nemčok J, Potfaj M, Rakús M, Vass D, Vozár J, Vozárová A (1996b) Geological map of Slovakia: Ministry of the environment of Slovak Republic. Geological Survey of Slovak Republic, Bratislava
- Black LP, Kamo SL, Allen CM, Aleinikoff JN, Davis DW, Korsch RJ, Foudoulis C (2003) TEMORA 1: a new zircon standard for Phanerozoic U–Pb geochronology. *Chem Geol* 200:155–170. doi:10.1016/S0009-2451(03)00165-7
- Brown SJ, Fletcher IR (1999) SHRIMP U–Pb dating of the pre-eruption growth history of zircons from 340 ka Whakamura ignimbrite, New Zealand: evidence for >250 k.y. magma resistance time. *Geology* 27:1035–1038
- Brown GC, Thorp RS, Webb PC (1984) The geochemical characteristic of granitoides in contrasting arcs and comments on magma source. *J Geol Soc Lond* 141:413–426
- Christiansen EH (2005) Contrasting processes in silicic magma chambers: evidence from very large volume ignimbrites. *Geol Magazine* 142:669–681
- Christiansen EH, McCurry M (2008) Contrasting origin of Cenozoic silicic volcanic rocks from the western Cordillera of the United States. *Bull Volcanol* 70:251–267

- Cordani UG, Teixeira W (2007) Proterozoic accretionary belts in the Amazonian Craton. *Geol Soc Am Mem* 200:297–320
- Cordani UG, Teixeira W, D'Agrella-Filho MS, Trindale RI (2009) The position of the Amazonian Craton in supercontinents. *Gondwana Res* 15:396–407
- Čorná O, Kamenický L (1976) Ein Beitrag zur Stratigraphie des Kristallinikums der Westkarpaten auf Grund der Palynology. *Geol Zborn Geol Carpath* 27:117–132
- Dallmayer RD, Neubauer F, Handler R, Fritz H, Müller W, Pana D, Putiš M (1996) Tectonothermal evolution of the internal Alps and Carpathians: evidence from $^{40}\text{Ar}/^{39}\text{Ar}$ mineral and whole rock data. *Eclogae Geol Helv* 89:203–227
- Dallmayer RD, Németh Z, Putiš M (2005) Regional tectonothermal events in Gemicum and adjacent units (Western Carpathians, Slovakia): contribution by $^{40}\text{Ar}/^{39}\text{Ar}$ dating. *Slovak Geol Mag* 11(2–3):155–163
- Faryad SW (1991) Metamorphism of the Early Paleozoic sedimentary rocks in the Gemicum. *Miner Slov* 23:315–324
- Faryad SW, Henjes-Kunst F (1997) K-Ar and $^{40}\text{Ar}/^{39}\text{Ar}$ constraints for the tectonothermal evolutions of the high-pressure Meliata Unit, Western Carpathians (Slovakia). *Tectonophysics* 280(4):141–156
- Fernández-Suárez J, Gutiérrez-Alonso G, Jeffries TE (2002) The importance of along-margin terrane transport in northern Gondwana: insights from detrital zircon parentage in Neoproterozoic rocks from Iberia and Brittany. *Earth Planet Sci Lett* 204:75–88
- Fernández-Suárez J, Gutiérrez-Alonso G, Pastor-Galán D, Hofmann M, Murphy JB, Linnemann U (2014) The Ediacaran–Early Cambrian detrital zircon record of NW Iberia: possible sources and paleogeographic constraints. *Int J Earth Sci (Geol Rundsch)* 103:1335–1357
- Finger F, Broska I (1999) The Gemic S-type granites in south-eastern Slovakia: late Paleozoic or Alpine intrusion? Evidence from electron-microprobe dating of monazite. *Schweiz Mineral Petrogr Mitt* 79:439–443
- Finger F, Broska I, Haunschmid B, Hraško L, Kohút M, Krenn E, Petrik I, Riegler G, Uher P (2003) Electron-microprobe dating of monazites from Western Carpathians basement granulites: plutonic evidence for an important Permian rifting event subsequent to Variscan crustal anatexis. *Int J Earth Sci (Geol Rundsch)* 92:86–98
- Gibson HL, Watkinson DH, Comba CDA (1983) Silicification: hydrothermal alteration in an Archean geothermal system within the Amulet Rhyolite Formation, Noranda, Quebec. *Econ Geol* 78:954–971
- Glazner AF, Coleman DS, Bartley JM (2008) The tenuous connection between high-silica rhyolites and granodiorite plutons. *Geology* 36:1047–1050
- Gorton MP, Schandl ES (2000) From continents to island arcs: a geochemical index of tectonic setting for arc-related and within plate felsic to intermediate volcanic rocks. *Can Mineral* 38:1065–1073
- Gutiérrez-Alonso G, Fernández-Suárez J, Jeffries TE, Jenner GA, Tubrett MN, Cox R, Jackson SE (2003) Terrane accretion and dispersal in the northern Gondwana margin. An Early Paleozoic analogue of a long-lived active margin. *Tectonophysics* 365:221–232. doi:10.1016/S0040-1951(03)00023-4
- Haas J (2001) Structural units and main stages of the structural evolution. In: Haas J (ed) *Geology of Hungary*. Eotvos University Press, Budapest, pp 19–22
- Henderson BJ, Collins WJ, Murphy JB, Gutiérrez-Alonso G, Hand M (2015) Gondwanan basement terranes of the Variscan–Appalachian orogen: Baltican, Saharan and West African hafnium fingerprints in Avalonia, Iberia and the Armorican Terranes. *Tectonophysics*. doi:10.1016/j.tecto.2015.11.020
- Heumann A, Davies GR (1997) Isotopic and chemical evolution of the post-caldera rhyolitic system at Long Valley, California. *J Petrol* 38:1661–1678
- Iizuka T, Campbell IH, Allen CM, Gill JB, Maruyama S, Makoka F (2013) Evolution of the African continental crust as recorded by U–Pb, Lu–Hf and O isotopes in detrital zircons from modern rivers. *Geochim Cosmochim Acta* 107:96–120
- International Commission on Stratigraphy. International Chronostratigraphic Chart v 2016/04). <http://www.stratigraphy.org/ICSChart/ChronostratChart2016-04.pdf>
- Ivan P (1994) Early Paleozoic of the Gemic Unit (Inner western Carpathians): geodynamic setting as inferred from metabasalts geochemistry data. *Mitt Öst Geol Gesell* 86:3–31
- Ivanička J, Snopko L, Snopková P, Vozárová A (1989) Gelnica Group, Lower unit of the Spišsko-gemerské rudohorie Mts. (Early Paleozoic, West Carpathians). *Geol Zborn Geol Carpath* 40:195–219
- Janik T, Grad M, Guterch A, Vozár J, Bielik M, Vozárová A, Hegedüs E, Kovács CA, Kovács I (2011) Crustal structure of the Western Carpathians and Pannonian Basin: seismic model from CEL-EBRATION 2000 data and geological implications. *J Geodyn* 52:97–113
- Jenner GA, Dunlapp GR, Malpas J, Brown M, Brace T (1991) Bay of Islands and Little Port complexes revisited: age, geochemical and isotopic evidence confirm supra-subduction-zone origin. *Can J Earth Sci* 28:1635–1652
- Jeřábek P, Faryad WS, Schulmann K, Lexa O, Tajčmanová L (2008) Alpine burial and heterogeneous exhumation of Variscan crust in the West Carpathians insight from thermodynamic and argon diffusion modelling. *J Geol Soc Lond* 165:479–498. doi:10.1144/0016-76492006-165
- Johnson MC, Plank T (1999) Dehydration and melting experiments constrain the fate of subducted sediments. *Geochem Geophys Geosyst* 1, Paper #1999GC000014
- Kohút M, Stein H (2005) Re–Os molybdenite dating of granite-related Sn–W–Mo mineralisation at Hnilec, Gemic Superrunit, Slovakia. *Mineral Petrol* 85:117–129. doi:10.1007/s00710-005-0082-8
- Kuznetsov NB, Natapov I, Belousova EA, O'Reilly SY, Griffin WL (2010) Geochronological, geochemical and isotopic study of detrital zircon suites from late Neoproterozoic clastic strata along the NE margin of the East European Craton: implications for plate tectonic models. *Gondwana Res* 17:583–601
- Larionov AN, Andreichev VA, Gee DG (2004) The Vendian alkaline igneous suite of northern Timan: ion microprobe U–Pb zircon ages of gabbros and syenite. In: Gee DG, Pease VL (eds) *The Neoproterozoic Timanide Orogen of eastern Baltica*. *Geol Soc Lond Mem* 30:69–74
- Lexa O, Schulmann K, Ježek J (2003) Cretaceous collision and indentation in the West Carpathians: view based on structural analysis and numerical modeling. *Tectonics* 22(6):1066. doi:10.1029/2002TC001472
- Linnemann U, Herbolch A, Liégeois J-P, Pin C, Gärtner A, Hofmann M (2012) The Cambrian to Devonian odyssey of the Brabant Massif within Avalonia: a review with new zircon ages, geochemistry, Sm–Nd isotopes, stratigraphy and paleogeography. *Earth Sci Rev* 112:126–154
- Linnemann U, Gerdes A, Hofmann M, Marko L (2014) The Cadomian orogen: Neoproterozoic to Cambrian crustal growth and orogenic zoning along peripheral of the West African Craton—constraints from U–Pb zircon ages and Hf isotopes (Schwarzbürg Antiform, Germany). *Precambrian Res* 244(214):236–278
- Ludwig KR (2005a) SQUID 1.12 A User's Manual. A Geochronological Toolkit for Microsoft Excel. Berkeley Geochronology Center Special Publication. pp 22. <http://www.bgc.org/klprogramm.html>

- Ludwig KR (2005b) User's Manual for ISOPLOT/Ex 3.22. A Geochronological Toolkit for Microsoft Excel. Berkeley Geochronology Center Special Publication. pp 71. <http://www.bgc.org/klprogrammenu.html>
- Ludwig KR (2012) Isoplot 3.75, A geochronological Toolkit for Microsoft Excel, Berkeley Geochronology Centre, Special Publication No. 5, rev January 30, 2
- MacLean WH (1990) Mass change calculations in altered rock series. *Miner Depos* 25:44–49
- Mahel M (1986) Geological structure of the Czechoslovak Carpathians, Part 1: Palealpine units. Monograph. Veda Publishing House, Bratislava, p 503 (in Slovak)
- Maluski H, Rajlich P, Matte P (1993) $^{40}\text{Ar}/^{39}\text{Ar}$ dating of Inner Carpathians Variscan basement and Alpine mylonitic overprinting. *Tectonophysics* 223:213–337
- Matteini M, Junges SL, Dantas EL, Pimentel MM, Bühn B (2010) In situ zircon U–Pb and Lu–Hf isotope systematic on magmatic rocks: insights on the crustal evolution of the Neoproterozoic Goiás Magmatic Arc, Brasília belt, central Brazil. *Gondwana Res* 17:1–12
- Matura A, Császár G, Kröll A, Vozár J, Wessely G (2000) Map of pre-Tertiary basement. Danube Region Environmental Geology Program, DANREG: Explanatory Notes, Jahrbuch GBA, Band 142/4:465–482
- McDonough WF, Sun S-S (1995) The composition of the Earth. *Chem Geol* 120:228
- McLennan SM (2001) Relationships between the trace element composition of sedimentary rocks and upper continental crust. *Geochim Geophys Geosyst*. doi:10.1029/2000GC000109
- Meinhold G, Kostopoulos D, Frei D, Himmerkus F, Reischmann T (2010) U–Pb LA–SF–ICP–MS zircon geochronology of the Serbo-Macedonian Massif, Greece: paleotectonic constraints for Gondwana-derived terranes in the Eastern Mediterranean. *Int J Earth Sci (Geol Rundsch)* 99:813–832
- Molák B, Buchardt B (1996) Stable isotope composition of carbon in selected carbonaceous units of Slovakia with reference to Úrkút (Hungary) and Copperbelt (Zambia) examples. *Slovak Geol Mag* 1:27–43
- Murphy JB, Nance RD (1989) Model for evolution of the Avalonian–Cadomian belt. *Geology* 17:735–738
- Murphy JB, Pisarevsky S, Nance RD (2013) Potential geodynamic relationship between the development of peripheral orogens along the northern margin of Gondwana and the amalgamation of West Gondwana. *Mineral Petrol* 107:635–650
- Nance RD, Murphy JB (1994) Contrasting basement signatures and palinspastic restoration of peripheral orogens: an example from the Neoproterozoic Avalonian–Cadomian belt. *Geology* 22:617–620
- Nance RD, Murphy JB, Strachan RA, Keppie JD, Gutiérrez-Alonso G, Fernández-Suárez J, Quesada C, Linnemann U, D'Lemos R, Pisarevsky SA (2008) Neoproterozoic–early Paleozoic tectonostratigraphy and paleogeography of the peri-Gondwanan terranes: Amazonian versus West African connections. *Geol Soc Lond Spec Publ* 297:345–383
- Neubauer F, Frisch W, Hansen BT (2002) Early Paleozoic tectonothermal events in basement complexes of the eastern Greywacke Zone (Eastern Alps): evidence from U–Pb zircon data. *Int J Earth Sci (Geol Rundsch)* 91:775–786
- Pearce JA (1983) Role of subcontinental lithosphere in magma genesis at active continental margin. In: Hawkesworth CJ, Norry MJ (eds) *Continental basalts and Mantle xenoliths*. Shiva, Nantwich, pp 230–249
- Pearce JA (1996a) A User's Guide to basalt Discrimination diagrams In: Wymann DA (ed) *Trace element geochemistry of Volcanic rocks: applications for massive Sulphide exploration*. Geo Assoc Canada, Short Course Note v 12 pp 79–113
- Pearce JA (1996b) Sources and settings of granitic rocks. *Episodes* 19(4):120–125
- Pearce JA, Peate DW (1995) Tectonic implications for the composition of volcanic arc magmas. *Annu Rev Earth Planet Sci* 23:251–285
- Pidgeon RT (1992) Recrystallisation of oscillatory zoned zircon: some geochronological and petrological implications. *Contrib Mineral Petrol* 110:463–472
- Piercey SJ, Nelson JL, Colpron M, Dusel-Bacon C, Simard R-L, Roots CF (2006) Paleozoic magmatism and crustal recycling along the ancient Pacific margin of North America, northern Cordillera. In: Colpron M, Nelson JL (eds) *Paleozoic Evolution and Metallogeny of Pericratonic Terranes at Ancient Pacific Margin of North America, Canadian and Alaskan Cordillera*. Geol Assoc Canada, Spec Pap 45: 281–322
- Pimentel MM, Rodrigues JB, DellaGiustina MES, Junges S, Matteini M, Armstrong R (2011) The tectonic evolution of the Neoproterozoic Brasilia Belt, central Brazil, based on SHRIMP and LA-ICPMS–U–Pb sedimentary provenance data. *Rev J South Am Earth Sci* 31:345–357
- Plašienka D, Grecula P, Putiš M, Kováč M, Hovorka D (1997) Evolution and structure of the Western Carpathians: an overview. In: Grecula P, Hovorka D, Putiš M (eds) *Geological evolution of the Western Carpathians*. Mineralia Slovaca Monograph, Bratislava, pp 1–24
- Putiš M, Sergeev S, Ondrejka M, Larionov M, Siman P, Spišiak J, Uher P, Paderin I (2008) Cambrian–Ordovician metaigneous rocks associated with Cadomian fragments in the Western Carpathians basement dated by SHRIMP on zircons: a record from the Gondwana active margin setting. *Geol Carpath* 59:3–18
- Putiš M, Frank W, Plašienka D, Siman P, Sulák M, Biroň A (2009) Progradation of the Alpidic orogenic wedge related to two subductions: constrained by $^{40}\text{Ar}/^{39}\text{Ar}$ ages of white mica. *Geodin Acta* 22(1–3):31–56. doi:10.3166/ga.22.31-56
- Radvanec M, Konečný P, Ondrejka M, Putiš M, Uher P, Németh Z (2009) Gemic granites as an indicator of the crustal extension above the Late Variscan subduction zone and during the Early Alpine riftingogenesis (Western Carpathians): an interpretation from monazite and zircon ages dated by CHIME and SHRIMP methods. *Miner Slov* 41:381–394 (in Slovak, English summary)
- Rakús M, Potfaj M, Vozárová A (1998) Basic paleogeographic and paleotectonic units of the Western Carpathians. In: Rakús M (ed) *Geodynamic development of the Western Carpathians*. D. Štúr Publ, Bratislava, pp 15–26
- Rogers JJW, Santosh M (2002) Configuration of Colombia, a Mesoproterozoic supercontinent. *Gondwana Res* 5:5–22
- Sassi FP, Vozárová A (1987) The pressure character of the Hercynian metamorphism in the Gemicum (West Carpathians, Czechoslovakia). *Rend Soc Ital Min Petrol* 42:73–81
- Schaltegger U, Nägler TF, Corfu F, Maggetti M, Galetti G, Stoch HG (1997) A Cambrian island arc in the Silvretta nappe: constraints from geochemistry and geochronology. *Schweiz Mineral Petrogr Mitt* 73:337–350
- Scotese CR (2004) A continental drift flipbook. *J Geol* 152:729–749
- Sisson TW (1994) Hornblende–melt trace-element partitioning measured by ion microprobe. *Chem Geol* 117:331–344
- Snopko L (1967) Lithological characteristics of the Gelnica Serie. *Západné Karpaty Sér Geol* 7:103–152 (in Slovak)
- Snopko L, Ivanička J (1978) Consideration about paleogeography of the Early Paleozoic rocks of the Spišsko gemerské rudohorie Mts. In: Vozár J, Mišík M, Marschalko R (eds) *Paleogeographic development of the Western Carpathians*. D Štúr Inst Geol, Bratislava, pp 269–279 (in Slovak, English summary)
- Snopková P, Snopko L (1979) Biostratigraphy of Gelnica Serie in the Spišsko-gemerské rudohorie Mts. based on palynological study. *Západné Karpaty Sér Geol* 5:57–102 (in Slovak)

- Soták J, Vozárová J, Ivanička J (1999) New microfossils from the Early Paleozoic formations of the Gemericum. *Geol Carpath* 50(Spec Iss):72–74
- Stampfli GM, Borel GD (2002) A plate tectonic model for Paleozoic and Mesozoic constrained by dynamic plate boundaries and restored synthetic oceanic isochrones. *Earth Planet Sci Lett* 196:17–33
- Steiger RH, Jäger E (1977) Subcommittee on geochronology: convention on the use of decay constants in geo- and cosmochronology. *Earth Planet Sci Lett* 36:359–362
- Sun S-S, McDonough WF (1989) Chemical and isotope systematic of oceanic basalts implications for mantle composition and processes. In: Saunders AD, Norry MJ (eds) *Magmatism in ocean basins*. *Geol Soc Lond Spec Publ* 42:313–345
- Talavera C, Montero P, Bea F, González Lodeiro F, Whitehouse M (2013) U–Pb zircon geochronology of the Cambro–Ordovician metagranites and detrital zircon geochronology of central and NW Iberia. *Int J Earth Sci (Geol Rundsch)* 102:1–23. doi:10.1007/s00531-012-0788-x
- Thompson MD, Barr SM, Grunow AM (2012) Avalonian perspectives on Neoproterozoic paleogeography: evidence from Sm–Nd isotope geochemistry and detrital zircon geochronology in SE New England, USA. *Bull Geol Soc Am* 124:517–531
- Ustaömer PA, Ustaömer T, Gerdes A, Zulauf G (2011) Detrital zircon ages from a Lower Ordovician quartzite of the Istanbul exotic terrane (NW Turkey): evidence for Amazonian affinity. *Int J Earth Sci (Geol Rundsch)* 100:23–41. doi:10.1007/s00531-009-0498-1
- vonRaumer JF, Bussy F, Schaltegger V, Schultz B, Stampfli GM (2013) Pre-Mesozoic Alpine basement—their place in the European Paleozoic framework. *Geol Soc Am Bull* 125:89–108
- Vozár J, Tomek Č, Vozárová A, Dvořáková V (1995) Deep seismic profile G: Geological interpretation (Inner Western Carpathians). *Spec Publ Geol Soc Greece*, 4(1), XVth Congress of CBGA, Athens, pp 34–37
- Vozárová A (1993a) Variscan metamorphism and crustal evolution of the Gemericum. *Západné Karpaty Sér Min Petr Geoch Metalog* 16:55–117 (in Slovak, English summary)
- Vozárová A (1993b) Provenance of Gelnica Group metasandstones and relationship to paleotectonic of the sedimentary basin. *Západné Karpaty Sér Min Petr Geoch Metalog* 16:5–54 (in Slovak, English summary)
- Vozárová A, Ivanička J (1996) Geodynamic setting of the Gelnica Group acid volcanism. *Slovak Geol Mag* 3–4:245–250
- Vozárová A, Soták J, Ivanička J (1998) A new microfauna from the Early Paleozoic of the Gemericum (foraminifera): constrains for another fossils or subfossils. In: Rakús M (ed) *Geodynamic development of the Western Carpathians*. *D Štúr Publ, Bratislava*, pp 63–74
- Vozárová A, Konečný P, Vozár J, Šmelko M (2008) Upper Jurassic–Lower Cretaceous tectonothermal events in the Southern Gemeric Permian rocks deduced from electron microprobe dating of monazite (Western Carpathians, Slovakia). *Geol Carpath* 59:89–102
- Vozárová A, Šmelko M, Paderin I (2009) Permian single crystal U–Pb zircon age of the Rožňava Formation volcanites (Southern Gemeric Unit, Western Carpathians, Slovakia). *Geol Carpath* 60(6):439–448. doi:10.2478/v10096-009-0032-1
- Vozárová A, Šarinová K, Larionov A, Presnyakov S, Sergeev S (2010) Late Cambrian/Ordovician magmatic arc volcanism in the Southern Gemeric basement, Western Carpathians, Slovakia: U–Pb (SHRIMP) data from zircon. *Int J Earth Sci (Geol Rundsch)* 99(Suppl 1):17–37. doi:10.1007/s00531-009-0454-0
- Vozárová A, Šarinová K, Rodionov N, Laurinc D, Paderin I, Sergeev S, Lepekhina E (2012) U–Pb ages of detrital zircons from Paleozoic metasandstones of the Gelnica Terrane (Southern Gemeric Unit, Western Carpathians, Slovakia): evidence for Avalonian–Amazonian provenance. *Int J Earth Sci (Geol Rundsch)* 101:919–936. doi:10.1007/s00531-011-0705-8
- Vozárová A, Konečný P, Šarinová K, Vozár J (2014) Ordovician and Cretaceous tectonothermal history of the Southern Gemeric Unit from microprobe monazite geochronology (Western Carpathians, Slovakia). *Int J Earth Sci (Geol Rundsch)* 103:1005–1022. doi:10.1007/s00531-014-1009-6
- Walsh GJ, Benziane F, Alejniov JN, Harrison RW, Yazidi A, Burton WC, Quick JE, Saadane A (2012) Neoproterozoic tectonic evolution of the Jebel Saghro and Bou Azzer-El Graara inliers, eastern and central Anti-Atlas, Morocco. *Precambrian Res* 216–219:23–62
- Wiedenbeck M, Alleé P, Corfu F, Griffin WL, Meier M, Oberli F, Von Quadt A, Roddick JC, Spiegel W (1995) Three natural zircon standards for U–Th–Pb, Lu–Hf, trace element and REE analyses. *Geostand Newsl* 19:1–23
- Williams IS (1998) U–Th–Pb Geochronology by ion microprobe. Applications in microanalytical techniques to understanding mineralizing processes. *Rev Econ Geol* 7:1–35
- Winchester JA, Floyd PA (1977) Geochemical discrimination of different magma series and their differentiation products using immobile elements. *Chem Geol* 20:325–343
- Winchester JA, Pharaoh TC, Verniers J, Ioane D, Seghedi A (2006) Paleozoic accretion of Gondwana-derived terranes of the East European Craton: recognition of detached terrane fragments dispersed after collision with promontories. In: Gee DG, Stephenson R (eds) *European lithosphere dynamics*. *Geol Soc Lond Mem vol 32*. pp 323–332
- Wood DA, Joron JL, Treuil M (1979) A re-appraisal of the use of trace elements to classify and discriminate between magma series erupted in different tectonic settings. *Earth Planet Sci Lett* 45:326–336
- Zhao G, Cawood PA, Wilde SA, Sun M (2002) Review of global 2.1–1.8 Ga orogens: implication for a pre-Rodinia supercontinent. *Earth Sci Rev* 59:125–162